HHS Public Access

Author manuscript

Neuron. Author manuscript; available in PMC 2020 December 04.

Published in final edited form as:

Neuron. 2019 December 04; 104(5): 960–971.e7. doi:10.1016/j.neuron.2019.08.042.

TREK-1 and TRAAK are principal K^+ channels at the nodes of Ranvier for rapid action potential conduction on mammalian myelinated afferent nerves

Hirosato Kanda[1], **Jennifer Ling**[1], **Sotatsu Tonomura**[1], **Koichi Noguchi**[2], **Sadis Matalon**[1], **Jianguo G. Gu**[1,*]

[1]Department of Anesthesiology and Perioperative Medicine, School of Medicine, University of Alabama at Birmingham, Birmingham, Alabama, 35294, USA

[2]Department of Anatomy and Neuroscience, Hyogo College of Medicine, Nishinomiya, Hyogo, 663-8501, Japan

Abstract

Rapid conduction of nerve impulses are critical in life and rely on action potential (AP) leaps through the nodes of Ranvier (NRs) along myelinated nerves. While NRs are the only sites where APs can be regenerated during nerve conduction on myelinated nerves, ion channel mechanisms underlying the regeneration and conduction of APs at mammalian NRs remain incompletely understood. Here we show that TREK-1 and TRAAK, the thermosensitive and mechanosensitive two-pore domain potassium (K2P) channels, are clustered at NRs of rat trigeminal Aβ-afferent nerves with density over 3000-fold higher than that on their somas. These K2P channels, but not voltage-gated K^+ channels as in other parts of nerves, are required for rapid AP repolarization at the NRs. Furthermore, these channels permit high-speed and high-frequency AP conduction along the myelinated afferent nerves, and loss of function of these channels at NRs retards nerve conduction and impairs sensory behavioral responses in animals.

In Brief

Kanda et al. studied ion channels at the nodes of Ranvier (NRs) on rat myelinated afferent nerves. They discovered that thermally sensitive K2P channels including TREK-1 and TRAAK are clustered at NRs to secure high-speed and high-frequency nerve conduction.

Graphical Abstract

*Leading Contact: Jianguo G. Gu, M.B., Ph.D., Department of Anesthesiology and Perioperative Medicine, School of Medicine, University of Alabama at Birmingham, Birmingham, Alabama, 35294, USA, jianguogu@uabmc.edu.

AUTHOR CONTRIBUTIONS

JGG conceived and designed the experiments and wrote the paper. KN conceived experiments of immunostaining. HK performed experiments and data analysis. JL and ST performed experiments for the revised manuscript. SM participated result interpretation and discussions.

DECLARATION OF INTERESTS

The authors declare no competing interests.

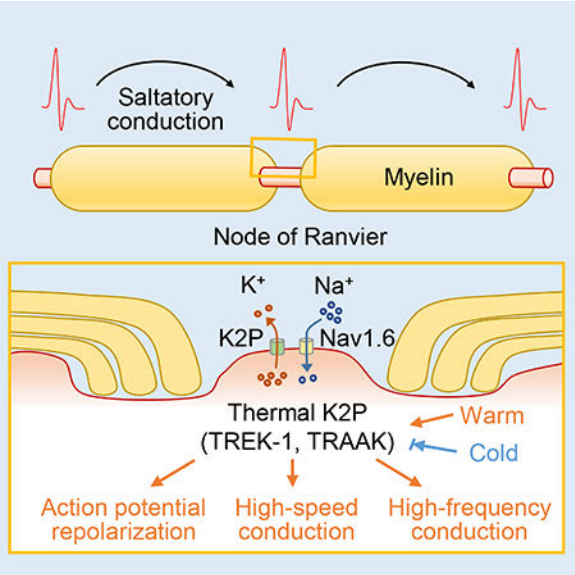

Keywords

Myelinated nerve; node of Ranvier; action potential; saltatory conduction; leak K^+ currents; two-pore domain K^+ channels; temperature; sensory; conduction velocity

INTRODUCTION

Rapid conduction of nerve impulses is achieved by action potentials (APs) leaping along myelinated nerves via the nodes of Ranvier, the tiny myelin-sheath gaps on myelinated nerves (Boullerne, 2016; Huxley and Stampfli, 1949; Lillie, 1925; Ranvier, 1871; Ranvier, 1872; Tasaki, 1939). AP propagation on myelinated nerves, also known as saltatory (hop or leap in Latin) conduction (Huxley and Stampfli, 1949; Lillie, 1925; Tasaki, 1939), can reach speeds over 100 m/s and frequencies over hundreds of hertz, 100 times more rapid than impulse conduction on unmyelinated nerves in mammals (Waddell and Lawson, 1990). Saltatory conduction ensures timely sensory responses with high acuity and rapid muscle movement with fine control. Impairments of saltatory conduction at NRs occur in many neurological diseases, including multiple sclerosis, spinal cord injury, and inflammatory demyelinating polyneuropathy (Arancibia-Carcamo and Attwell, 2014; Devaux et al., 2012; Stathopoulos et al., 2015; Waxman, 1992, 2006), leading to sensory and motor dysfunctions. NRs are the only places where APs are regenerated to permit saltatory conduction, and voltage-gated Na^+ channels clustered at NRs (Caldwell et al., 2000; Ritchie and Rogart, 1977) are partially responsible for the AP regeneration by driving AP depolarization. However, the ion channels responsible for driving rapid AP repolarization at NRs and for securing high-speed as well as high-frequency AP conduction on mammalian myelinated nerves remain to be unknown.

Regeneration of APs at NRs of myelinated nerves has long been thought to be the same mechanistically as that on the other parts of nerves, i.e., AP depolarization is driven by voltage-gated Na^+ channels and AP repolarization driven mainly by voltagegated K^+

channels (Bean, 2007). This classical ion channel mechanism is responsible for AP regeneration at amphibian NRs (Hucho et al., 1976). However, in mammalian species including rats and rabbits, Chiu and Ritchie failed to detect significant amount of K^+ currents at intact NRs except when the myelin sheaths of the nerves were loosen chemically (Chiu and Ritchie, 1980), and they suggested that K^+ channels may be not present at NRs for AP regeneration. On the other hand, Binah and Palti detected large K^+ currents at NRs of rat myelinated nerves (Binah and Palti, 1981). Since then, there have been long debates whether or not K^+ channels are present at NRs for AP repolarization and conduction. This fundamental issue remains unsolved because patch-clamp recordings, the most appropriate technique for addressing this question, has never been successfully applied to intact NRs of mammalian myelinated nerves. Much of our knowledge about ion channels at mammalian NRs is based on immunohistochemical studies, which provides useful but limited information about the functions of ion channels at NRs. Immunohistochemical studies on mammalian NRs have shown that voltage-gated Na^+ channel Nav1.6 and Nav1.2 are clustered at NRs (Caldwell et al., 2000; Waxman, 2006). These voltage-gated Na^+ channels are believed to drive action potential depolarization during saltatory conduction. Voltage-gated K^+ channel Kv7.2 (Devaux et al., 2004) and Kv3.1b (Devaux et al., 2003) were also detected in mammalian NRs and Kv1.1 as well as Kv1.2 were detected in juxtaparanodal regions immunohistochemically (Rhodes et al., 1997). However, presently there is no information as whether these voltage-gated K^+ channels at NRs or juxtaparanodal regions are involved in action potential repolarization at NRs. Subsequently, alternative hypotheses have been proposed for AP repolarization at NRs such as inactivation of voltage-gated Na^+ channels and/or a periaxonal K^+ pathways (Barrett and Barrett, 1982; Li, 2015; Rash et al., 2016). However, none of these putative mechanisms have been tested functionally with the patch-clamp recording technique.

A more important issue about NRs is whether and how ion channels at NRs may play a key role in securing saltatory conduction at high-speed and high-frequency. Very few studies have investigated mechanisms responsible for high-frequency AP conduction on myelinated nerves. For high-speed AP conduction on myelinated nerves, previous studies have mainly focused on effects of myelination on conduction velocity (Castelfranco and Hartline, 2016). Interestingly, based on studies with computational modeling, it has been hypothesized that the speed of membrane charge for AP initiation at NRs may be a rate-limiting factor for saltatory conduction (Castelfranco and Hartline, 2015, 2016). Biophysically, the speed of membrane charge is faster with smaller membrane capacitance and also with larger membrane input conductance. Intriguingly, myelinated axons are substantially narrowed at each NR, a structural feature thought to be an evolutionary change to reduce membrane capacitance thereby to increase the speed of membrane charge at NRs (Castelfranco and Hartline, 2016; Halter and Clark, 1993). However, a reduction in nodal membrane areas with narrowed nodal axons would normally result in a substantial decrease of membrane input conductance, which would slow membrane charge at NRs (Moore et al., 1978). Nevertheless, if the narrowed nodal axon is co-evolved with the clustering of ion channels that substantially increase membrane input conductance at NRs, this would greatly increase the speed of nodal membrane charge and provide a novel mechanism to secure high-speed AP conduction through NRs in myelinated nerves (Castelfranco and Hartline, 2015, 2016;

Halter and Clark, 1993). This putative mechanism has so far never been tested experimentally since, except voltage-gated Na^+ channels, no other principal ion channels have been identified at NRs of mammalian myelinated nerves.

Two-pore domain K^+ (K2P) channels are a family of 15 members that were originally known as “leak” or “background” K^+ channels (Enyedi and Czirjak, 2010; Goldstein et al., 2005; Lotshaw, 2007). K2P channels are distinct from voltage-gated K^+ channels in their structure, biophysical and pharmacological properties, and electrophysiological functions. K2P channels are expressed at low levels on neurons and are involved in setting membrane input conductance and resting membrane potentials (Enyedi and Czirjak, 2010). Of the 15 K2P subtypes, TREK-1, TREK2, and TRAAK are 3 closely related subtypes displaying both thermal and mechanical sensitivity (Enyedi and Czirjak, 2010; Kang et al., 2005; Kim et al., 2001; Maingret et al., 2000; Maingret et al., 1999). K2P channels in neurons have been suggested to play roles in regulation of excitability, sensory transduction, and neuroprotection (Lotshaw, 2007). Mutations in K2P channels such as TRAAK missense mutations result in abnormal functions of central and peripheral nervous systems in humans (Bauer et al., 2018). TREK channels have recently been found to be inhibited by migraine-associated TRESK mutations to result in neuronal hyperexcitability (Royal et al., 2019). However, it is entirely unknown whether any K2P channels may be highly expressed at NRs of mammalian myelinated nerves and if so, whether they play a critical role in regeneration and rapid conduction of APs at NRs. Here we developed an *in situ* pressure-patch-clamp recording technique and using a rat *ex vivo* trigeminal nerve preparation, we made patch-clamp recordings at intact NRs of mammalian myelinated nerves for the first time. Using this key technique in combination with immunohistochemical, genetic and pharmacological approaches, and *in vivo* sensory behavioral assessments, we have addressed these key questions.

RESULTS

Nodes of Ranvier of myelinated afferent nerves display unconventional action potentials and high leak K^+ conductance

Whole-cell patch-clamp recording is the most direct approach to study ion channels and their potential functions in saltatory conduction at NRs, but has never been applied to an intact NR of mammalian myelinated nerves due to technical challenges. This is because NRs are tiny axonal segments surrounded by tough perineural tissues, which not only makes it impossible to visualize nodal axons but also prevents recording electrodes from forming quality membrane seals for patch-clamp recordings. Structural intact of NRs is essential in the present study since a structural alteration at NRs such as demyelination could alter ion channels and impair saltatory conduction (Waxman, 2006). We developed an *in situ* pressure-patch-clamp recording technique, and for the first time directly made patch-clamp recordings at intact NRs of trigeminal Aβ-afferent nerves in a rat *ex vivo* trigeminal afferent nerve preparation (Fig. 1A&B, Fig. S1). The *in situ* pressure-patch-clamp recording technique relied on a pressure-clamp device to help patch-clamp electrodes to approach tiny invisible nodal axons and to facilitate the formation of cell-attached and whole-cell patch-clamp recording modes (Fig. S1). This new recording technique allowed us for the first time

to investigate the function of ion channels at NRs in saltatory conduction. Using recording electrodes that contained fluorescent dye Alexa-555, we also were able to trace and characterize the morphological properties of nodal, paranodal and inter-nodal axons of the fresh trigeminal Aβ-afferent nerves recorded under the whole-cell patch-clamp configuration (Fig. 1B, Table S1). Nodal and paranodal axons were much narrower than inter-nodal axons and had diameters of ~ 1.88 μm and total length of ~ 4.2 μm, and inter-nodal axons had diameters of ~ 5.4 μm and length of ~736 μm (Fig. 1B, Table S1). The much narrowed axonal segments at NRs shown in our rat trigeminal Aβ-afferent nerves resemble the structural feature commonly seen in myelinated axons of peripheral nerves in mammals (Castelfranco and Hartline, 2016).

By using patch-clamp recordings at NRs of trigeminal Aβ-afferent nerves, our first finding was that APs at NRs were unconventional in that AP repolarization was totally independent of voltage-gated K^+ channels. This was evidenced by the lack of effects on AP repolarization (AP width) by high concentrations of extracellular TEA (20 mM) plus intracellular Cs^+ (135 mM), two blockers of voltage-gated K^+ channels (Fig. 1C). For conventional APs such as those recorded at somas of trigeminal Aβ-afferent nerves, AP repolarization largely depends on voltage-gated K^+ channels and blocking these channels with TEA plus Cs^+ retarded AP repolarization and severely prolonged AP widths (Fig. 1D). Thus, repolarization of APs at NRs of myelinated afferent nerves are mechanistically distinct from classical APs generated at other places in neuronal cells, a finding that settles the decade-long controversies on the mechanisms of AP repolarization in mammalian myelinated nerves (Barrett and Barrett, 1982; Li, 2015; Rash et al., 2016).

We next examined ionic currents at NRs of trigeminal Aβ-afferent nerves to provide insights into the unconventional APs. The direct whole-cell patch-clamp recordings at intact NRs allowed us for the first time to quantitatively determine ionic currents and their characteristics at NRs of the myelinated afferent nerves. Large and transient inward currents were evoked following voltage steps and the inward currents were completely blocked by tetrodotoxin (TTX, Fig. S2), consistent with the clustering of the voltage-gated Na^+ channels Nav1.6 at NRs required for driving AP depolarization during saltatory conduction (Caldwell et al., 2000; Waxman, 2006). A striking finding following the depolarizing voltage steps was the appearance of strong non-inactivating outward currents which were not significantly inhibited by voltage-gated K^+ channel blockers 135 mM Cs^+ (intracellular) plus 20 mM TEA (Fig. 1E) or the Kv7.2 inhibitor linopirdine (Fig. S2). In contrast, in the somas of trigeminal Aβ-afferent nerves non-inactivating outward currents were largely inhibited by Cs^+ plus TEA (Fig. S3). Thus, different from other parts of nerves where voltage-gated K^+ channels mediate most of outward currents (Bean, 2007), voltage-gated K^+ channels did not significantly contribute to the outward currents at intact NRs of myelinated afferent nerves. This result is consistent with the lack of significant effects on APs by voltage-gated K^+ channel blockers at NRs of trigeminal Aβ-afferent nerves (Fig. 1C).

Since the non-inactivating outward currents at NRs were the most prominent ionic currents whose nature was completely unknown, we next determined the ionic basis of the outward currents at NRs of trigeminal Aβ-afferent nerves. Outward currents of a cell could be mediated by influx of Cl^- ions through membrane Cl^- channels. However, the outward

currents at NRs were not due to Cl^- ion influx via Cl^- channels since the outward currents were not affected when altering Cl^- concentrations or applying Cl^- channel blockers (Fig. S4). Nevertheless, altering extracellular K^+ concentrations shifted the reversal potentials, consistent with Goldman-Hodgkin-Katz equation for K^+-permeable channels (Fig. 1F). Thus, the outward currents at the NRs fell into the class of "leak" or "background" K^+ currents (IK_{leak})(Enyedi and Czirjak, 2010; Goldstein et al., 2005; Lotshaw, 2007). In contrast to NRs, non-inactivating outward currents in the somas of trigeminal Aβ-afferent nerves were mainly mediated by classical voltage-gated K^+ channels since they were largely inhibited by Cs^++TEA (Fig. S3). Remaining outward currents in the presence of the voltage-gated K^+ channel blockers, which should be mostly IK_{leak} currents, were small in the somas of trigeminal Aβ-afferent nerves (Fig. S3).

The presence of IK_{leak} currents on nodal membranes was not surprising since IK_{leak} currents would be needed for generating resting membrane potentials at NRs. However, what was very surprising was the huge IK_{leak} currents detected at nodal membranes of trigeminal Aβ-afferent nerves. Considering a nodal axon being 1.88 μm in diameter and 1.78 μm in length (Table S1) and its nerve soma being a sphere with diameter of 50 μm, the density of the IK_{leak} currents at NRs of trigeminal Aβ-afferent nerves was estimated to be over 3000 fold higher than that of the IK_{leak} currents at their somas. We made single channel recordings from nodal membranes under the cell-attached mode, and identified a major type of unitary IK_{leak} currents with a large single channel conductance of 93 ± 5 pS at 80 mV and 118 ± 6 pS at −80 mV (n = 15), and weak inward rectification (Fig. 1G). Thus, NRs of trigeminal Aβ-afferent nerves have unusually high leak K^+ conductance mediated by large-conductance leak K^+ channels.

Leak K^+ conductance at the nodes of Ranvier of myelinated afferent nerves are thermosensitive and mechanosensitive and identified as TREK-1 and TRAAK channels

The unexpectedly large IK_{leak} currents at NRs of trigeminal Aβ-afferent nerves led us to further investigate molecular identities mediating these currents at NRs. K2P channels, a family of at least 15 members, have been cloned and shown to be responsible for mediating IK_{leak} currents (Enyedi and Czirjak, 2010; Goldstein et al., 2005; Lotshaw, 2007). However, none of these K2P channels have been reported to be present at NRs. To determine if members of K2P channels may mediate the large IK_{leak} currents at NRs, we tested the thermal sensitivity of IK_{leak} currents at NRs. This is because TREK-1, TREK-2 and TRAAK, a sub-family of K2P channels have large single channel conductance and are thermally sensitive. The whole-cell IK_{leak} currents increased at 35°C and decreased at 15°C and 10°C comparing to controls at 24°C (Fig. 2A&B), indicating that they are thermally sensitive channels. Expressed as IK_{leak} conductance, i.e., the slopes of I-V curves near the holding voltages (−72 to −82 mV), the changes of IK_{leak} were highly significant at different temperatures (Fig. 2C). Consistent with the whole-cell IK_{leak} currents, the single channel event numbers and open probability were also temperature-dependent (Fig. 2D–F, n = 6). Cloned TREK-1, TREK-2 and TRAAK channels are mechanosensitive (Lotshaw, 2007). IK_{leak} single channel currents recorded at NRs were significantly increased in their numbers and probabilities of channel openings in responses to negative pressures (Fig. 2G–I, n = 6), indicating that the IK_{leak} channels are mechanosensitive.

Immunoreactivity to TREK-1 (TREK-1-ir) and to TRAAK (TRAAK-ir), but not to TREK-2 (TREK-2-ir), was observed in the axonal regions of trigeminal Aβ-afferent nerves lacking myelin basic protein (MBP) immunoreactivity (Fig. 3A–C). Furthermore, TREK-1-ir or TRAAK-ir on trigeminal Aβ-afferent nerves was present between the immunoreactivity of contactin associated protein 1 (CASPR), a glycoprotein specifically enriched in paranodal axonal regions (Fig. 3A&B, Fig. S5). The specificity of the antibodies for TREK-1 and TRAAK were validated using their blocking peptides (Figure S5) and also validated by the specific immunoreactivity to TREK-1 and TRAAK heterologously expressed in HEK293 cells (Figure S6). TREK-1 immunoreactivity but not TRAAK immunoreactivity was also observed at NRs of the myelinated nerve fibers in the spinal dorsal column, ventral column and motor nerves (Fig. S7). For trigeminal Aβ-afferent nerves, 87% and 91 % of their nodes were TREK-1-ir and TRAAK-ir positive, respectively (Fig. 3D), indicating that TREK-1 and TRAAK are mostly co-expressed at NRs of myelinated afferent nerves.

The co-expression of TREK-1 and TRAAK at NRs of trigeminal Aβ-afferent nerves raised a question as whether they formed heteromeric TREK-1/TRAAK channels. Previous studies have shown that mouse TREK-1 and TRAAK each formed homomeric channels and their co-expression formed heteromeric channels (Blin et al., 2016; Levitz et al., 2016). However, a recent study has shown that TREK-1 and TRESK form heteromeric channels in trigeminal neurons and that the activity of these channels are potentiated by intracellular Ca^{2+} elevation (Royal et al., 2019). Nevertheless, we found that IK_{leak} currents at NRs were not affected by the Ca^{2+} ionophore ionomycin (Fig S8), suggesting that functional K2P channels at NRs of trigeminal Aβ-afferent nerves are unlikely to be heteromeric channels formed by TREK-1 and TRESK. We expressed rat TREK-1 in HEK293 cells, which resulted in homomeric TREK-1 channels with single channel conductance of 67 ± 6 pS (n = 6) at 80 mV and 88 ± 10 pS (n = 5) at −80 mV (Fig. 3E, F&H). We also expressed TRAAK in HEK239 cells, which resulted in homomeric TRAAK channels with single channel conductance of 100 ± 12 pS (n = 6) at 80 mV and 67 ± 12 pS (n = 6) at −80 mV (Fig. 3E, F&H). In contrast, when TREK-1 and TRAAK channels were co-expressed, a new type of unitary currents appeared which had single channel conductance of 87 ± 7 pS (n = 5) at 80 mV and 125 ± 6 pS (n = 8) at −80 mV (Fig. 3E, G&H). The new channels are distinct from the homomeric channels formed by either TREK-1 or TRAAK (Fig. 3E–H), indicating that co-expression of TREK-1 and TRAAK proteins resulted in the formation of heteromeric TREK-1/TRAAK channels. In the HEK293 cells co-transfected with TREK-1 and TRAAK, we also observed a single channel type with conductance of 51 ± 3 pS at 80 mV (n = 5) and 87 ± 4 pS at −80 mV (n = 12), similar to homomeric TREK-1 channels (TREK-1-like, Figure 3G&H). For the heteromeric TREK-1/TRAAK channels formed in HEK293, their single channel conductance was similar to the single channels recorded at the NRs (Nodal K2P, Fig. 3H). In HEK293 cells co-expressed both TREK-1 and TRAAK, whole-cell patch-clamp recordings showed large outward currents following depolarizing voltage steps and the currents were temperature-sensitive and TEA-insensitive (Fig. S9), similar to the whole-cell IK_{leak} currents recorded at NRs (Fig. 1&2). Homomeric TREK-1 channels expressed in HEK293 cells were also not sensitive to TEA or to Zn^{2+} (Fig. S9). Thus, at NRs of trigeminal Aβ-afferent nerves functional leak K^+ channels were most likely formed as heteromeric TREK-1/TRAAK

channels but the presence of homomeric TREK-1 and homomeric TRAAK cannot be excluded.

TREK-1 and TRAAK channels are required for rapid action potential repolarization at the node of Ranvier of myelinated afferent nerves

To explore the role of TREK-1 and TRAAK channels at NRs of myelinated afferent nerves, we designed shRNAs to knockdown TREK-1 and TRAAK channels. The shRNAs were inserted in adeno-associated viral (AAV) plasmids containing eGFP or mCherry reporter genes, packed into AAV particles, and microinjected into maxillary (V2) branches of trigeminal afferent nerves (Fig. 4A). After 4 weeks, eGFP and mCherry were observed in trigeminal afferent nerve somas (Fig. S10) and their peripheral axons (Fig. 4B). In whole-cell patch-clamp recordings, shTREK-1-expressing and shTRAAK-expressing NRs of trigeminal Aβ-afferent nerves showed significantly smaller IK_{leak} conductance comparing with shScramble group (Fig. 4C&D). A greater reduction of IK_{leak} conductance, by approximately 30%, was observed with shTREK-1+shTRAAK double knockdown (Fig. 4C&D). Consistently, in eGFP-positive trigeminal afferent nerve somas, strong TREK-1 immunoreactive neurons were significantly less in shTREK-1 group than in shScramble group (Fig. S10); in mCherry-positive trigeminal afferent nerve somas, strong TRAAK immunoreactive neurons were significantly less in shScramble group than in shTRAAK group (Fig. S10). Pharmacologically, IK_{leak} currents at NRs were also significantly inhibited by barium (Ba^{2+}), norfluoxetine (NF), and ruthenium red (RR) (Fig. 4E), three IK_{leak} channel inhibitors (Lotshaw, 2007). In contrast, BL1249 (BL), intracellular arachidonic acid (AA), and intracellular low pH of 5 ($[pH]_i$ 5), three activators of thermosensitive and mechanosensitive K2P channels (Lotshaw, 2007), significantly potentiated IK_{leak} currents at 24°C (Fig. 4F) and 15°C (Fig. S11).

TREK-1 and TRAAK channels may play a pivotal role in driving rapid AP repolarization at the NRs of myelinated afferent nerves. To test this hypothesis, we determined whether AP repolarization at NRs may be retarded by gene knockdown or pharmacological inhibition of TREK-1 and TRAAK channels. AP repolarization at NRs of trigeminal Aβ-afferent nerves was rapid with AP widths of ~0.7 ms (Fig. 4G). However, AP widths at NRs were significantly prolonged in shTREK-1, shTRAAK, or shTREK-1+shTRAAK groups, which decreased TREK-1, TRAAK, or both TREK1 and TRAAK, respectively (Fig. 4G). AP widths at NRs were also significantly prolonged following Ba^{2+}, NF and RR applications to inhibit the leak K^+ channels (Fig. 4H). We performed AP-dynamic clamp recordings at NRs and showed that AP repolarization phase was aligned with the outward currents, and the outward currents were insensitive to the voltage-gated K^+ channel blocker TEA (Fig. 4I) but were inhibited by Ba^{2+} which blocked lK_{leak} currents (Fig. 4J). These results further support the role of leak K^+ channels in driving rapid AP repolarization at NRs and suggest that TREK-1 and TRAAK channels are required for the formation of rapid APs at NRs of myelinated afferent nerves for saltatory conduction.

Knockdown and pharmacological inhibition of TREK-1 and TRAAK channels also increased nodal membrane input resistance, and depolarized resting membrane potentials (Table S2), but had no effects on voltage-activated sodium currents at NRs of trigeminal Aβ-

afferent nerves (Fig. S12). The effects on nodal membrane input resistance and resting membrane potentials (Table S2) also revealed a role of TREK-1 and TRAAK channels in controlling intrinsic membrane properties. The very negative resting membrane potentials at NRs of trigeminal Aβ-afferent nerves (near −82 mV, Table S2) were thus a result of the high expression of TREK-1 and TRAAK channels.

TREK-1 and TRAAK channels are required for high-frequency and high-speed saltatory conduction on myelinated afferent nerves and for *in vivo* sensory behavioral responses

Sensory information is encoded by nerve impulses in a broad range of frequencies up to hundreds of hertz, and TREK-1 and TRAAK channels at NRs may be critical for high-frequency impulses conducted on myelinated afferent nerves. To test this idea, we first compared APs conducted through somas and through NRs of trigeminal Aβ-afferent nerves following increased stimulation frequencies (Fig.5A&B). At somas where voltage-gated K^+ channels drive AP repolarization, APs were broadened in a frequency-dependent manner (Fig. 5B). In sharp contrast, action potentials showed no AP broadening at NRs of trigeminal Aβ-afferent nerves in response to high frequency stimulation up to 200 Hz (Fig. 5B). We next examined AP success rates at different stimulation frequency. APs conducted through somas typically failed at frequencies ≥ 50 Hz and mostly failed at 200 Hz (Fig. 5C, Fig. S13). In contrast, APs conducted through NRs of trigeminal Aβ-afferent nerves showed no significant failures at frequencies up to 200 Hz (Fig. 5C, Fig. S13). Quantitatively described by the frequency at which AP conduction success rate was 50% (FS_{50}), FS_{50} was 74.2 ± 23.7 Hz (n = 6) and 458.1 ± 58.3 (n = 7) Hz for APs conducted through somas and NRs, respectively (Fig. 5C, Fig. S13). AP success rates at NRs were significantly reduced in shTREK-1, shTRAAK, and shTREK-1 +shTRAAK groups (Fig. 5D, Fig. S14). Similarly, AP success rates at NRs were significantly reduced by Ba^{2+}, NF and RR that inhibit the IK_{leak} currents (Fig. 5E, Fig. S14). These results indicate that TREK-1 and TRAAK channels play a key role in high-frequency AP conduction on mammalian myelinated afferent nerves.

TREK-1 and TRAAK channels may be required for high-speed nerve conduction along myelinated afferent nerves. To test this hypothesis, we determined whether AP conduction velocity at NRs of trigeminal Aβ-afferent nerves was reduced following knockdown of TREK-1 and/or TRAAK channels. AP conduction velocity recorded at NRs of trigeminal Aβ-afferent nerves was 48.3 ± 1.8 m/s (n = 6) in control group injected with shScramble, and was significantly reduced to 30.4 ± 1.9 m/s (n = 6), 28.5 ± 1.6 m/s (n = 6) and 24.5 ± 0.7 m/s (n = 6) in shTREK-1, shTRAAK and shTREK-1+shTRAAK groups, respectively (Fig. 6A&B). Consistently, AP conduction velocity at NRs of trigeminal Aβ-afferent nerves was also significantly reduced following the applications of Ba^{2+}, NF and RR to inhibit the K2P channels at NRs (Fig. 6C). These results indicate that TREK-1 and TRAAK channels at NRs play a key role in securing high-speed AP conduction on mammalian myelinated afferent nerves. Conduction velocity was also progressively reduced with temperature decreases from 35°C to 15°C (Fig. 6D), consistent with the inhibition of IK_{leak} currents at NRs at cooling temperatures (Fig. 2A–B). Furthermore, BL, AA and intracellular pH of 5, three activators of thermosensitive and mechanosensitive K2P channels, reversed the cold-induced reduction of AP conduction velocity (Fig. 6E). The conduction velocity recorded at NRs was

not affected in the presence of a mixture of voltage-gated K^+ channel blockers TEA (20 mM), Cs^+(135 mM, intracellular), and 4-AP (1 mM, intracellular) (Fig. 6F). These results indicated that high-speed nerve conduction along myelinated afferent nerves relies on the activity of TREK-1 and TRAAK channels at NRs.

The role of TREK-1 and TRAAK channels in AP conduction on myelinated afferent nerves should impact *in vivo* sensory behavioral responses. To test this idea, tactile behavioral tests were performed in animals (Fig. 6G) that were microinjected with the aforementioned shRNA-AAV preparations into individual D2 whisker hair follicles (Fig. 6H) or individual D2 whisker afferent nerves (Fig. 6I). Four weeks following the microinjections of the shRAN-AAV preparations, animals were tested in a blinded manner for their avoidance behaviors in responses to tactile stimulation to whisker hairs (Fig. 6G). The reason for the use of the whisker tactile behavioral tests was because impulses elicited by tactile stimuli are conducted by trigeminal Aβ-afferent nerves. As shown in Figure 6H&I, microinjection of the shRNAs-AAV preparations into D2 whisker hair follicles (Fig. 6H) or into D2 whisker afferent nerves (Fig. 6I) to knockdown TREK-1 and TRAAK channels resulted in a significant reduction of tactile responses in comparison with the scrambled shRNA control group (shScramble). These results suggested that TREK-1 and TRAAK channels at NRs of myelinated afferent nerves are essential for *in vivo* sensory behavioral responses, and loss of function of these channels at NRs impairs *in vivo* sensory behavioral responses.

DISCUSSION

In this study we have shown that TREK-1 and TRAAK are principal ion channels clustered at NRs of myelinated afferent nerves of rats. These thermosensitive and mechanosensitive K2P channels, not classical voltage-gated K^+ channels as in other parts of nerves, drive rapid AP repolarization at NRs of myelinated afferent nerves. More importantly, we have demonstrated that these K2P channels at NRs are required for high-speed and high-frequency saltatory conduction along myelinated afferent nerves as well as *in vivo* tactile behavioral responses.

By applying our newly developed *in situ* pressure-patch-clamp recording technique to intact NRs of trigeminal Aβ-afferent nerves, we have detected for the first time large leak K^+ currents and measured their current density at NRs of the myelinated afferent nerves. The density of leak K^+ currents is over 3000 times higher at nodal membranes than at soma membranes of trigeminal Aβ-afferent nerves. This indicates that leak K^+ channels are specifically clustered and anchored at mammalian NRs of myelinated afferent nerves as principal ion channels. The leak K^+ channels at NRs of trigeminal Aβ-afferent nerves are the thermosensitive and mechanosensitive K2P channels most likely formed by TREK-1 and TRAAK. This conclusion is based on several lines of evidence including the presence of immunoreactivity of TREK-1 and TRAAK at the NRs of trigeminal Aβ-afferent nerves, the whole-cell currents and single channel properties recorded from the nodal membranes, and pharmacology and gene knockdown experiments. Immunostaining results of the present study indicated that most NRs of trigeminal Aβ-afferent nerves co-expressed both TREK-1 and TRAAK channels. We show that the co-expression of rat TREK-1 and TRAAK in HEK293 cells resulted in the formation of heteromeric TREK-1/TRAAK channels, with

electrophysiological properties consistent with previous studies with mouse TREK-1 and TRAAK channels (Blin et al., 2016). At the NRs of trigeminal Aβ-afferent nerves, single channel properties of our nodal K2P channels suggest that these channels may be heteromeric TREK-1/TRAAK channels. The clustering of high density TREK-1 and TRAAK channels at NRs of trigeminal Aβ-afferent nerves may require anchoring proteins, the nature of which has not been determined in the current study. Ankyrin-G and neurofascin have been shown to be anchoring proteins for the clustering of high density voltage-gated Na^+ channels at NRs (Arancibia-Carcamo and Attwell, 2014; Jenkins et al., 2015). Nodal anchoring proteins may enrich K2P channels such that their immunoreactivity is detectable at NRs but may or may not be detectable at their somas. It should be noted that TREK-1 but not TRAAK was detected immunochemically at NRs of motor nerves as well as central projection nerves in the spinal dorsal and ventral columns, raising the possibility that TREK-1 may be functional K2P channels clustered at NRs of these myelinated nerves.

At NRs of trigeminal Aβ-afferent nerves the high density leak K^+ currents mediated by TREK-1 and TRAAK channels well matches the high density voltage-gated Na^+ channels at NRs (Arancibia-Carcamo and Attwell, 2014; Jenkins et al., 2015). This can permit sufficiently large outward currents flowing through the leak K^+ channels to rapidly drive AP repolarization at NRs. This pivot role of TREK-1 and TRAAK channels in AP regeneration at the NRs of myelinated afferent nerves is evidenced by significant prolongation of AP widths following gene knockdown or pharmacological inhibition of these channels. Thus, the NR of myelinated afferent nerves is a unique site on an afferent neuron where leak K^+ channels rather than conventional voltage-gated K^+ channels drive action potential repolarization. It should be noted that in the present study under the condition with gene knockdown or pharmacological inhibition, AP repolarization was significantly retarded but not completely impaired. This partial effect on AP repolarization may be due to the partial suppression of the activity of TREK-1 and TRAAK channels under our experimental conditions with gene knockdown or pharmacological inhibition. In addition, inactivation of voltage-gated Na^+ channels at NRs may also partially contribute to AP repolarization. Previous immunochemical studies have shown the expression of the voltage-gated K^+ channel Kv7.2 (Devaux et al., 2004) at NRs and the expression of Kv1.1 and Kv1.2 in juxtaparanodal regions (Rhodes et al., 1997) of mammalian peripheral nerves. However, outward currents carried by these voltage-gated K^+ channels may be too small to be detected in the present study due to the overwhelmingly large outward currents carried by leak K^+ channels. The contribution of voltage-gated K^+ channels to AP repolarization at intact NRs may be also too small to be detected in the present study. The functions of these channels in saltatory conduction are not the scope of the present study, but previous studies have proposed that these nodal and extra-nodal voltage-gated K^+ channels may fine tune the excitability of nodal axons (Zhou et al., 1999). In addition, these voltage-gated K^+ channels may be upregulated to compensate the loss of function of K2P channels at NRs in mice with the global deletion of TREK-1, TREK-2, and TRAAK genes (Mirkovic et al., 2012). However, K2P channels are better suited than voltage-gated K^+ channels to drive AP repolarization and regeneration at NRs of myelinated afferent nerves since these leak K^+ channels activate and inactivate nearly instantaneously (Renigunta et al., 2015).

We have shown that TREK-1 and TRAAK channels at NRs are essential in securing saltatory conduction at high-frequency on myelinated afferent nerves. Several mechanisms may underlie this important role of these leak K^+ channels. First, with the use of the leak K^+ channels for AP repolarization, each AP at NRs is brief and frequency-dependent AP broadening (Liu et al., 2017) will not take place at NRs. Second, instantaneous channel activation and deactivation of K2P channels (Renigunta et al., 2015) minimizes inter-spike interval. Third, the very negative resting membrane potentials due to high leak K^+ conductance at NRs should promote a quick recovery of voltage-gated Na^+ channels from inactivation following each action potential (Bean, 2007). These effects collectively would permit saltatory conduction at high-frequency through NRs of myelinated afferent nerves.

TREK-1 and TRAAK channels at NRs are shown in the present study to be essential for saltatory conduction at high-speed along myelinated afferent nerves. This important role of the leak K^+ channels may be due to the enhanced nodal membrane input conductance or the decreased nodal membrane input resistance, a result from the clustering of the high-density TREK-1 and TRAAK channels at NRs. Previous theoretical studies by computational modeling have predicted that addition of ion channels to enhance membrane input conductance at NRs would accelerate membrane charge at NRs and boost the speed of saltatory conduction (Castelfranco and Hartline, 2015, 2016; Halter and Clark, 1993). Our study for the first time provides experimental evidence supporting this novel mechanism responsible for securing high-speed saltatory conduction on mammalian myelinated afferent nerves. Thus, NRs are not only the sites of AP regeneration during saltatory condition, but also are sites controlling the speed of AP conduction on myelinated afferent nerves in mammals.

We show that temperature sensitivity of TREK-1 and TRAAK channels at the NRs of myelinated afferent nerves significantly contribute to temperature-dependent saltatory conduction with conduction velocity reduced in colder temperatures (Franz and Iggo, 1968). TREK-1 and TRAAK channels are more sensitive to temperature changes than voltage-gated Na^+ channels are (Hodgkin and Huxley, 1952; Kang et al., 2005; Maingret et al., 2000). Therefore, these thermosensitive and mechanosensitive K2P channels may account more for temperature-dependent saltatory conduction than voltage-gated Na^+ channels do. We show that cooling temperatures impair saltatory conduction by inhibiting the thermosensitive and mechanosensitive K2P channels at the NRs of myelinated afferent nerves. This finding may have clinical implications for sensory impairment such as numbness in cold temperatures in patients with peripheral neuropathy.

Our *in vivo* tactile behavioral assessments performed in a blinded manner demonstrate the impairment of tactile sensory responses in animals following the knockdown of TREK-1 and TRAAK channels in whisker afferent nerves. The tactile behavioral assessments is well suited for the present study since impulses evoked by whisker displacements are conducted by trigeminal Aβ-afferent nerves. These impulses are generated from several different types of low threshold mechanoreceptors including rapidly adapting types and slow adapting types in whisker hair follicles (Gottschaldt et al., 1973). All impulses generated from these low threshold mechanoreceptors are conducted at high-speed on trigeminal Aβ-afferent nerves, and impulses generated from slowly adapting types of low threshold mechanoreceptors in

whisker hair follicles are conducted at high-frequency (Chang et al., 2016; Ikeda et al., 2014). Therefore, it is conceivable that knockdown of TREK-1 and TRAAK channels which compromises rapid saltatory conduction on the trigeminal Aβ-afferent nerves would impair the *in vivo* tactile behavioral responses.

The use of K2P channels for rapid AP conduction may represent an evolutionary advancement to permit high-frequency and high-speed saltatory conduction on myelinated afferent nerves of mammals. It is conceivable that this advancement may be widely adopted in mammalian nervous systems including other rapidly conducting somatosensory afferent nerves, motor nerves, and ascending and descending projection nerves in the central nervous system. Consistently, we have found that TREK-1 channels are not only clustered at NRs of myelinated afferent nerves, but also highly expressed at NRs of motor nerves as well as central projection nerves in the spinal dorsal and ventral columns. It remains to determine whether TREK-1 and/or other K2P channels are used for rapid AP conduction at NRs of all myelinated nerves in the peripheral and central nervous systems of mammals. Growing evidence has shown that molecular dysfunctions occur at NRs in many neurological diseases such as inflammatory demyelinating neuropathy (Devaux et al., 2012; Stathopoulos et al., 2015), multiple sclerosis (Waxman, 2006), and spinal cord injury (Waxman, 1992), leading to severe sensory and motor impairments. Loss of function of TREK-1 and TRAAK channels at NRs of myelinated afferent nerves in our animals impairs *in vivo* sensory behavioral responses. It would be interesting to study in future whether K2P channels at NRs of different myelinated nerves may be targeted by pathological factors such autoantibodies (Devaux et al., 2012; Stathopoulos et al., 2015) to impair nerve conduction leading to sensory and motor dysfunctions in humans.

STAR★METHODS

LEAD CONTACT AND MATERIALS AVAILABILITY

Further information and requests for resources and reagents should be directed to and will be fulfilled by the Lead Contact, Jianguo Gu (jianguogu@uabmc.edu). There are no restrictions on any data or materials presented in this paper.

EXPERIMENTAL MODEL AND SUBJECT DETAILS

Animals—Male Sprague-Dawley rats (Envigo, Prattville, AL, USA) aged at 5–7 weeks were used for experiments. The rats were housed in a temperature-controlled room (23°C) and maintained on a 12-hour light/dark cycle. Animal care and use conformed to NIH guidelines for care and use of experimental animals. Experimental protocols (IACUC-10249) were approved by the Institutional Animal Care and Use Committee at the University of Alabama at Birmingham. For knockdown of TREK-1 and TRAAK gene expression, a glass electrode with a tip size of 5 μm was filled with shRNA/AAV preparations for TREK-1 and/or TRAAK genes and inserted into the nerve bundle of infraorbital nerves or D2 whisker hair follicles. The shRNA/AAV preparations were then slowly microinjected into the nerve bundle or D2 whisker hair follicles. Control groups were microinjected with scrambled shRNA/AAV preparations.

METHOD DETAILS

***Ex vivo* trigeminal nerve preparation—**Rats were euthanized by overdose of isoflurane, and trigeminal nerve bundles (~15 mm) with their ganglia were dissected out and placed in a petri dish filled with ice cold Leibovitz's L-15 medium (Corning cellgro®, Manassas, VA, USA). Connective tissues on the surface of the nerves were removed with a fine forceps under a dissection microscope. Trigeminal nerve bundles with their ganglia were then affixed in a recording chamber by a tissue anchor and submerged in a normal Krebs solution that contained (in mM): 117 NaCl, 3.5 KCl, 2.5 $CaCl_2$, 1.2 $MgCl_2$, 1.2 NaH_2PO_4, 25 $NaHCO_3$, and 11 glucose. The Krebs solution was saturated with 95% O_2 and 5% CO_2, had pH of 7.35 and osmolarity of 324 mOsm, and at room temperature of 24°C. The recording chamber was mounted on the stage of an Olympus BX51 microscope that was equipped with IR-DIC and fluorescent imaging systems. To facilitate patch-clamp electrode to penetrate perineural tissues, the trigeminal nerve bundles were briefly exposed to a mixture of 0.07% dispase® II (Roche, Indianapolis, IN, USA) and 0.07% collagenase (MilliporeSigma, Billerica, MA, USA) in Krebs solution for 5 min at the room temperature, and the enzymes were then washed off with the Krebs solution. The *ex vivo* trigeminal nerve preparation was continuously perfused with Krebs bath solution at 24°C, unless otherwise indicated.

***In situ* pressure-patch-clamp recordings at nodes of Ranvier—**Nodes of Ranvier in myelinated nerves of *ex vivo* trigeminal nerve preparations were visualized under a 40x (NA 0.80) water immersion objective and with an infrared CCD camera (IR-1000, DAGE-MTI, USA). Myelinated nerves chosen for all experiments had diameters (including myelin thickness) of 8 to 10 μm. The axons at nodes of Ranvier for these myelinated nerves had diameters of ~2 μm. These myelinated nerves were Aβ-afferent nerve fibers based on their conduction velocity.

Patch-clamp recordings were performed at nodes of Ranvier of trigeminal Aβ-afferent nerve fibers. Recording electrodes were pulled with a Flaming/Brown Micropipette Puller (P-97, Shutter Instruments, CA, USA). The electrode resistance after filling recording electrode internal solutions ranged from 8 to 10 MΩ for patch-clamp recordings at nodes of Ranvier and from 5 to 6 MΩ for patch-clamp recordings from the somas of trigeminal ganglia. For most experiments, recording electrodes were filled with a K^+-based internal solution containing (in mM): 105 K-gluconate, 30 KCl, 0.5 $CaCl_2$, 2.4 $MgCl_2$, 5 EGTA, 10 HEPES, 5 Na_2ATP and 0.33 GTP-TRIS salt; the pH of the solution was adjusted to 7.35 with KOH. The use of high Cl^- intracellular solution was because trigeminal afferent nerves normally have high intracellular Cl^- concentrations. In some experiments, a Cs^+-based internal solution was used and the solution contained (in mM): 135 CsCl, 0.5 $CaCl_2$, 2.4 $MgCl_2$, 5 EGTA, 10 HEPES, 5 Na_2ATP and 0.33 GTP-TRIS salt; the pH of the solution was adjusted to 7.35 with CsOH. In the Cs^+-based internal solution, Cs^+ served as major intracellular cation and also as a blocker for voltage-gated K^+ channels. To access nodal axon membranes by recording electrodes and achieve high quality membrane seals, a high-speed pressure-clamp device (HSPC-1, ALA Scientific instruments, NY, USA) was connected to patch-clamp recording electrode to fine control internal pressures of patch-clamp recording electrodes. A high positive pressure of 200 mmHg was first applied into recording electrodes

to pressure-clean the surface areas around nodes of Ranvier. Intra-electrode positive pressures were then reduced to 80 to 100 mmHg while electrodes were penetrating the perineurium that wrapped on nodal axons. Once the recording electrodes penetrated through the perineurium, intra-electrode pressures were reduced to 5 mmHg to approach nodal axons. Since nodal axons could not be differentiated from perineural tissues under the IR-DIC microscope, optimally accessing nodal axon membranes was judged by the reduction of seal-test currents and the appearance of a small current oscillation. Once the electrode tip optimally assessed nodal membranes, intra-electrode positive pressure was gradually reduced and a negative pressure of −2 to −10 mmHg was applied into recording electrodes until forming gigaohm seals (usually > 5 GΩ) between the recording electrodes and nodal axon membranes (usually less than 3 min). To achieve whole-cell configuration, nodal membranes were ruptured by a train of short electrical pulses (±200 mV, 20 ms each pulse) delivered through the patch-clamp recording electrodes while intra-electrode pressures were held at a constant negative pressure of −30 mmHg. After establishing the whole-cell configuration, negative pressure was reduced to −5 mmHg and maintained during recordings. Stable recordings from nodes of Ranvier usually could last for more than 1 hour. For patch-clamp recordings from somas of trigeminal ganglia, cells with large diameters (~50 μm) were chosen because they were usually the somas of trigeminal Aβ-afferent nerves. High positive pressure of 200 mmHg was initially applied into the recording electrode during penetration through satellite glial cell layers that wrapped around individual somas of trigeminal nerves. Once penetrated through satellite glia layers, intra-electrode pressures were reduced to 20 mmHg to approach the somas of trigeminal ganglia. After achieving optimal contact between electrodes and membranes, a negative pressure of approximately −10 mmHg was applied until the formation of gigaohm seals. Signals of voltage-clamp experiments were recorded and amplified using an Axopach 200B amplifier, filtered at 2 kHz and sampled at 10 kHz using the pCLAMP 10 software (Molecular Devices, Sunnyvale, CA, USA). Signals of current-clamp recordings for action potentials at nodes of Ranvier were low-pass filtered at 2 kHz and sampled at 50 kHz.

To determine the properties of membranes and action potentials of nodal axons, patch-clamp recordings were performed under the whole-cell current-clamp configuration. Step current pulses were injected into nodes of Ranvier through recording electrodes. Step currents were from −100 pA to 1800 pA with increments of 50 pA per step and the duration of each pulse was 1 s. To determine the properties of currents flowing through nodal membranes following voltage steps, recordings were performed under the whole-cell voltage-clamp configuration with nodal membranes held at −72 mV. Voltage steps were applied from −102 mV to +58 mV (voltage command of −90 to +70 mV) with increments of 10 mV each step and a step duration of 500 ms. Unless otherwise indicated, membrane voltages mentioned in the texts have been corrected for the calculated junction potentials of 12 mV.

To record single channel activity of axonal membranes at nodes of Ranvier, the aforementioned *in situ* pressure-patch-clamp recordings were applied to nodes of Ranvier and recordings were performed under the cell-attached configuration. After forming gigaohm seal between patch-clamp recording electrodes and nodal membranes, intra-electrode pressure was adjusted to 0 mmHg using a high-speed pressure-clamp device. Single channel recordings were performed using K^+-base recording electrode internal

solution with the K^+ concentration being 135 mM, which yielded symmetrical K^+ concentrations across nodal membranes (assuming intra-nodal K^+ concentrations were approximately 135 mM). Therefore, the reversal potentials of single channels that were permeable to K^+ would be near 0 mV. Experiments were performed with nodal membranes voltage-clamped at the voltage steps from −80 mV to 80 mV with increments of 10 mV each step. The values of voltages in recoding electrodes were in reference to the resting membrane potentials of −80 mV at nodes of Ranvier. Single channel activity was recorded and amplified using Axopatch 200B amplifier and signals were low-pass filtered at 2 kHz and sampled at 10 kHz.

Determination of conduction velocity and success rates of action potential propagation through nodes of Ranvier of trigeminal Aβ-afferent nerves—To determine conduction velocity of action potentials through nodes of Ranvier of myelinated afferent nerves, action potentials were evoked at a peripheral end of the infraorbital nerve branch using a suction stimulation electrode. The suction stimulation electrode had its tip size about 1 mm in diameter and was fire-polished. The peripheral end of trigeminal afferent nerve (infraorbital branch) was aspirated into the suction stimulation electrode with a tight fitting by a negative pressure. The negative pressure was continuously applied into the suction stimulation electrode to maintain the tight fitting during experiments. To initiate action potentials at the peripheral end of the nerve, monophasic square wave pulses were generated by an electronic stimulator (Master-8, A.M.P.I, Israel) and delivered via a stimulation isolator (ISO-Flex, A.M.P.I, Israel) to the suction stimulation electrode. The duration of the stimulation pulse was 50 μs. Minimum stimulation intensity for evoking action potentials, i.e. stimulation threshold at the peripheral end of the nerves, was first determined. Then stimulation was applied at the intensity of 2 fold of threshold (3.52 ± 0.34 mA, n = 12) throughout the experiments. Conduction velocity was calculated based on the latency of action potentials and the length of axons. The latency of action potentials was measured from the time of stimulation that was marked by stimulation artifacts to the time when action potential was initiated at the nodal recording site. The length of axons was the distance between stimulation site and nodal recording site. In some cases, stimulation artifacts were not completely separated from action potentials due to short length of axons. In these cases, the time of action potential initiation was first resolved by subtraction of artifacts, and then the latency of action potentials was measured for determining conduction velocity. To determine success rates of action potentials at nodes of Ranvier following different stimulation frequencies, stimulation pulses were applied to the trigeminal nerve bundles at frequencies of 1, 10, 50, 100, 200, 500 and 1000 Hz. Stimulation at each frequency was applied for 20 s. Intervals between different tests were 30 s. Success rates of action potential conducted through nodes of Ranvier were the percentage of successfully propagated action potentials through the nodal recording sites during 20 s period of stimulation.

Thermal and mechanical sensitivity—Effects of temperatures on membrane and action potential properties at nodes of Ranvier as well as on conductions of action potentials along trigeminal Aβ-afferent nerves were determined by the aforementioned electrophysiological experiments at bath solution temperatures of 35, 24, 15 and 10°C. The

temperatures of bath solutions were controlled by a Peltier temperature control system (CL-200A, Warner Instrument, CT, USA), and were continuously monitored with a thermal probe placed in the recording chamber (TA-29, Warner Instrument, CT, USA). The bath solution was applied at 2 ml/min from a short tube (500 μm in internal diameter) whose outlet was positioned 1 cm away from the recording site. The time was less than 1 min for warming from 24°C to 35°C and less than 2 min for cooling f rom 24°C to 10°C at the recording site. Effects of mechanical stimulation on single channel activity of nodal membrane patches were determined by applications of stepwise negative pressures via patch-clamp recording electrodes. The stepwise pressure pulses were generated by the high-speed pressure-clamp device (HSPC-1, ALA Scientific instruments, NY, USA) that was connected to patch-clamp recording electrodes.

Short hairpin RNA (shRNA)/AAV preparations for knockdown of TREK-1 and TRAAK channels—The sequence of shRNAs for targeting a region of rat TREK-1 mRNA (shTREK-1) was 5'- CAAAGTGGAGGACACATTTAT-3', for targeting a region of rat TRAAK mRNA (shTRAAK) was 5'-ACCATCGGCTACGGCAATATA-3'. The scrambled sequence of shRNA that does not target any known rat genes (shScramble) was 5'-CCTAAGGTTAAGTCGCCCTCG-3' and was used as control. The sequences of shTREK-1 and shScramble were separately inserted into the adeno-associated viral (AAV) vectors which contain human U6 promoter to drive shRNA expression and a reporter gene for the expression of enhanced green fluorescent protein (eGFP). The sequence of shTRAAK was inserted into the AAV vectors which contain human U6 promoter to drive shTRAAK expression and a reporter gene for the expression of mCherry fluorescent protein (mCherry). The above vector constructors were packed in either adeno-associated virus serotype 5 (AAV5, for shTREK-1 and shTRAAK) or serotype 2 (AAV2, for shScramble). All the above mentioned shRNA/AAV preparations were custom-prepared by VectorBuilder Inc. (Santa Clara, CA, USA) and the titer of each preparation was > 10^{12} viral particles.

Delivery of shRNA/AAV preparations to trigeminal afferent nerves—Rats were anesthetized with isoflurane and the anesthesia was maintained by continuous administration of isoflurane via a nose cone using an isoflurane anesthesia machine (E-Z Anesthesia, Euthanex Corp., PA, USA). The skin along top of the snout was shaved and a mid-line incision was made to expose nasal and maxillary bone. Infraorbital nerve was exposed 1 mm rostral to infraorbital fissure in the maxillary bone by using a pair of forceps. A glass electrode with a tip size of 5 μm was filled with shRNA/AAV preparations. The electrode was then mounted on an injection holder of a stereotaxic apparatus. Under a dissection microscope, the glass electrode was inserted into the nerve bundle of infraorbital nerves. The shRNA/AAV preparations were then slowly microinjected into the nerve bundle using a microprocessor-controlled pump (Micro4, World Precision Instruments, Fl, USA). Each shRNA/AAV preparation was microinjected at the volume of 3 μl, and the duration of each injection was 2 min and the glass microelectrode remained within the nerve bundle for 10 min before being withdrawn. The microinjections were performed on both sides of infraorbital nerves in each rat. Four weeks after the administration of shRNA/AAV preparations, trigeminal nerves with their ganglia were dissected out from rats. Patch-clamp recordings were then performed at nodes of Ranvier of eGFP-expressing or mCherry-

expressing myelinated afferent nerve fibers. Some of these rats were fixed with 4% PFA 4 weeks after microinjections of shRNAs/AAV and immunohistochemistry experiments were then performed on their trigeminal nerves and ganglia. In a different set of experiments, the shTREK-1/AAV and shTRAAK/AAV preparations or shScramble/AAV (control) were microinjected into D2 whisker hair follicles in a similar manner as aforementioned intra-nerve microinjections.

Whisker tactile behavioral assessments—Four weeks after microinjections of the shRNA/AAV preparations into infraorbital nerves or D2 whisker hair follicles, whisker tactile behavioral responses were assessed. Whisker tactile behavioral assessments were performed in a blinded manner in which the examiner did not know the shScamble group and the group microinjected with shTREK-1/AAV and shTRAAK/AAV. In brief, rats were placed in a cage and habituated for 10 min. During habituation and subsequent experiments, the testing room only had a red light on so that animals could not see the examiners and the tactile stimulation filament (300 g von Frey filament, Touch Test, USA). After the habituation, a single whisker hair (right side D2 whisker) was displaced (strike-through in 1 s) in ventral-dorsal direction by the tactile stimulation filament, and the whisker tactile test was performed 30 times with an interval of ~30 s between trials. The tactile responses were quantified by two methods. One method is based on response scores in that no response is 0, sniffing 1, avoiding head movement 2, avoiding body movement 3. Another one is the percent of the above tactile responses induced by tactile stimulation.

Pharmacology—Electrophysiological properties of nodes of Ranvier were tested with the following pharmacological reagents. Tetraethylammonium (TEA, 20 mM, MilliporeSigma, Billerica, MA, USA), cesium (Cs^+, MilliporeSigma, Billerica, MA, USA, 135 mM applied intracellularly, replacing K^+ in the recording electrode internal solution) and 4-pyridinamine (4-AP, 1 mM, MilliporeSigma, Billerica, MA, USA) for blocking voltage-gated K^+ channels. Barium (Ba^{2+}, 5 mM, MilliporeSigma, Billerica, MA, USA), ruthenium red (RR, 2 μm, MilliporeSigma, Billerica, MA, USA), and norfluoxetine (NF, 50 μm, Cayman Chemical, MI, USA) for inhibiting leak K^+ channels. BL1249 (BL, 10 μm, Tocris Bioscience, Bristol, UK), arachidonic acid (AA, 20 μm, Tocris Bioscience, Bristol, UK) and intracellular low pH of 5 ($[pH]_i$ 5) for potentiating leak K^+ channel activity. Linopirdine (LP, 10 μm, MilliporeSigma, Billerica, MA, USA) for blocking Kv7.2 channels. These reagents were either applied through bath solution to the recording chambers (TEA, Ba^{2+}, RR, NF, and BL1249) or applied intracellularly through recording electrode internal solutions (Cs^+, AA, $[pH]_i$ 5). Cs^+ was applied in the Cs^+-based recording electrode internal solution that contained 135 mM Cs^+.

To determine K^+ permeability of leak currents recorded at nodes of Ranvier, currents following voltage steps (from −102 mV to +58 mV) were first recorded in normal Krebs solution and then recorded in a high K^+ bath solution. The high K^+ bath solution contained (in mM): 120.6 KCl, 2.5 $CaCl_2$, 1.2 $MgCl_2$, 1.2 NaH2PO4, 25 NaHCO3 and 11 glucose. The high K^+ bath solution and recording electrode internal solution had similar K^+ concentrations, which would shift reversal potentials to ~0 mV if the leak currents were carried by K^+ ions. To determine Cl^- permeability of leak currents, currents following

voltage steps (from −102 mV to +58 mV) were first recorded in normal Krebs solution and then recorded in a low Cl^- extracellular bath solution that contained (in mM): 29.9 NaCl, 87.1 sodium-gluconate, 3.5 KCl, 2.5 $CaCl_2$, 1.2 $MgCl_2$, 1.2 NaH_2PO_4, 25 $NaHCO_3$, and 11 glucose. With this low Cl^- bath solution, the Cl^- concentrations at extracellular and intracellular sides were symmetric with a ratio of 1:1, which would shift the reversal potentials to ~0 mV if the leak currents were carried by Cl^- ion. In a different set of experiments, a cocktail of Cl^- channel blockers was bath applied to test if leak currents were inhibited by Cl^- channel blockers. These experiments were performed under the voltage”clamp configuration in normal Krebs solution. The cocktail of Cl^- channel blockers contained 1 mM Zn^{2+} (MilliporeSigma, Billerica, MA, USA), 100 μm phoretin (MilliporeSigma, Billerica, MA, USA), and 500 μm 4,4’-Diisothiocyanato-2,2’-stilbenedisulfonic acid disodium salt (DIDS, Tocris Bioscience, Bristol, UK).

For all pharmacology tests with bath application of testing compounds, unless otherwise indicated, each compound was perfused to *ex vivo* nerve preparations for 10 min. The testing compounds were delivered through a pinch valve drug delivery system (VC-6, Warner Instrument, CT, USA) which was controlled by digital signals from pClamp 10 software. For experiments with intracellular applications of testing compounds, each compound was dissolved in recording electrode internal solutions and recordings were performed 20 min after establishing the whole-cell configuration.

Morphology of nodes of Ranvier and inter-nodal axons—To determine lengths and diameters of nodal axons and inter-nodal axons, axons were labeled by the fluorescent dye Alexa Fluor 555 (ThermoFisher Scientific, Waltham, MA, USA). The dye was applied through recording electrode internal solution that contained 85 μm Alexa Fluor 555. Following the establishment of the whole-cell configuration for 30 min, nodal and inter-nodal axons were visualized under a fluorescent microscope. The fluorescence excitation was provided by an LED illumination system (X-Cite 120LED, Lumen Dynamics, Mississauga, ON, Canada). A filter set with excitation wavelength of 500 – 550 nm and emission wavelength of 565 – 625 nm was used for imaging Alexa Fluor 555 fluorescence. The images of dye-labeled axons were captured with a digital complementary metal-oxide semiconductor (CMOS) camera (ORCA-Flash4.0 LT, Bridgewater, NJ, USA). The images were then analyzed using the ImageJ software (National Institutes of Health, Bethesda, USA) to measure the lengths and diameters of nodal, paranodal and inter-nodal axons.

Immunohistochemistry—Rats were anesthetized with isoflurane and perfused with 4% paraformaldehyde (PFA), and trigeminal afferent nerves with their ganglia were dissected out. After post-fixation in 4% PFA for 24 hours, tissues were then transferred to a solution of 30% sucrose in PBS for 2 days. Tissues were then rapidly frozen in powdered dry ice. Tissues were sectioned at the thickness of 10 μm each section at −20°C using a Leica CM1860 cryomicrotome (Leica Biosystems, Nusslock, Germany). The sections were washed in PBS 3 times each for 10 minutes, and then the sections were sequentially washed with 50%, 70% and 50% ethanol (made in distilled water) each for 10 minutes. Sections were washed again in PBS for 3 times each for 10 minutes. They were then incubated in a blocking solution of 10% normal goat serum in PBS for 30 min at room temperature. They

were further incubated with primary antibodies in dilution buffer (5% normal goat serum in PBS) overnight at 4°C. After w ashing the sections in PBS 3 times each 10 minutes, the sections were incubated with a secondary antibody in dilution buffer (5% normal goat serum in PBS) for 1 h at room temperature. Following 3 washes in PBS each for 10 minutes, anti-fade mountant (ProLong Diamond Antifade Mountant, Invitrogen, Carlsbad, CA, USA) was added and sections were covered by cover-glasses. Following primary antibodies were used: rabbit anti-K2P 2.1 (TREK-1, 1:1000 or 1:500, Alomone labs, Jerusalem, Israel), rabbit anti-K2P 10.1 (TREK-2, 1:1000, Alomone labs, Jerusalem, Israel), rabbit anti-K2P 4.1 (TRAAK, 1:1000 or 1:500, Alomone labs, Jerusalem, Israel), chicken anti-Myelin basic protein (1:1000, Abcam, Cambridge, MA, USA), mouse anti-contactin associated protein 1 (CASPR, 1:1000 or 1:500, MilliporeSigma, Burlington, MA, USA), chicken anti-GFP (1:2000, Aves Labs Inc., Tigard, OR, USA) and mouse anti-mCherry (1:2000, Abcam, Cambridge, MA, USA). The following secondary antibodies were used for visualizing the immunohistochemistry results. They were Alexa Fluor 594-conjugated goat anti-rabbit (1:1000, Invitrogen, Carlsbad, CA, USA), Alexa Fluor 488-conjygated goat anti-rabbit (1:1000, Invitrogen, Carlsbad, CA, USA), Alexa Fluor 488-conjugated goat anti-chicken (1:1000; Abcam, Cambridge, MA, USA) and Alexa Fluor 594-conjugated goat anti-mouse (1:1000, Invitrogen, Carlsbad, CA, USA). In a subset of immunostaining for TREK-1, TRAAK, and CASPR, trigeminal afferent nerves and spinal ventral root nerves (motor nerves) as well as spinal cords were dissected out. Tissues were then rapidly frozen in powdered dry ice. Tissues including trigeminal afferent nerves, motor nerves, and spinal dorsal and ventral columns were sectioned at the thickness of 10 μm each section at −20°C using a Leica CM1860 cryomicrotome. Sections were air dried for 6 min and fixed with −20°C acetone or −20°C methanol for 7 min and air dried for an additional 30 min. The sections were washed in PBS 3 times each for 10 minutes. They were then processed for blocking and other procedures described above. In a subset of experiment to validate the specificity of TREK-1 and TRAAK antibodies, the primary antibodies were pre-incubated with 5 times (by weigh) of their blocking peptides for overnight at 4°C. The pre-absorbed antibodies were then used for immunohistochemical experiments described above.

TREK-1 and TRAAK expression in HEK293 cells and electrophysiological characterization—Rat TREK-1 subunits (rKcnk2, NM_172042.1) were cloned into pRP[Exp]-eGFP-CMV plasmid and rat TRAAK subunits (rKcnk4, NM_053804.2) cloned into pRP[Exp]-mCherry-CMV plasmid for expression in HEK293 cells and electrophysiological characterization. HEK293 cells were grown on coverslips in 35-mm dish in 2 ml DMEM (Fisher Scientific, cat#10–013-CV) with 10% fetal bovine serum (Hyclone/Fisher Scientific, SH30071.02), 100 units/ml penicillin-streptomycin (Invitrogen, 15140–122). They were then transfected with the TREK-1 plasmid (1 μg per dish), the TRAAK plasmid (1 μg per dish), or the TREK-1 plasmid (1 μg per dish) plus TRAAK plasmid (1–5 μg per dish) using Lipofectamine 2000 reagent (Invitrogen, 11668–027) in 1 ml DMEM medium. Three to five days following the transfection, patch-clamp recordings were performed either under whole-cell or cell-attached configurations. During recordings cells were perfused with normal Krebs bath solution. Recording electrode internal solution contained 105 K-gluconate, 30 KCl, 0.5 $CaCl_2$, 2.4 $MgCl_2$, 5 EGTA, 10 HEPES, 5 Na_2ATP and 0.33 GTP-TRIS salt; the pH of the solution was adjusted to 7.35 with KOH.

QUANTIFICATION AND STATISTICL ANALYSIS

Electrophysiological data were measured using the Clampfit software (Molecular Devices, Sunnyvale, CA, USA). All data analyses were performed using the GraphPad Prism software (version 7, La Jolla, CA, USA). Data are presented as mean ± SEM. Unless otherwise indicated, statistical significance was evaluated using paired, unpaired Student's t-Test, one-way ANOVA with *Tukey's* post hoc tests, or Chi-square test. Differences were considered to be significant with $*p < 0.05$, $**p < 0.01$ and $***p < 0.001$, and not significant (ns) with $p \geq 0.05$. Sample sizes of each experimental group and methods of data analysis were chosen based on standards in the field, and no tests were applied to predetermine sample sizes. All error bars indicate standard error of mean (SEM) unless indicated otherwise in the Figure Legends. Each figure Legend lists the number of recordings or number of animals used in each experiment group and the statistical tests used.

DATA AND CODE AVALABILITY

The published article includes all datasets generated or analyzed during this study. All data are available from the Lead Contact upon request.

ADDITIONAL RESOURCES

Not Applicable

Supplementary Material

Refer to Web version on PubMed Central for supplementary material.

ACKNOWLEDGMENTS

We thank Drs. Amy MacDermott, Jacques Wadiche, and Kevin Harrod for comments on an earlier version of this manuscript. This work was supported by NIH grants DE018661, DE023090, and NS109059 to J.G.G.

References

Arancibia-Carcamo IL, and Attwell D (2014). The node of Ranvier in CNS pathology. Acta Neuropathol 128, 161–175. [PubMed: 24913350]

Barrett EF, and Barrett JN (1982). Intracellular recording from vertebrate myelinated axons: mechanism of the depolarizing afterpotential. J Physiol 323, 117–144. [PubMed: 6980272]

Bauer CK, Calligari P, Radio FC, Caputo V, Dentici ML, Falah N, High F, Pantaleoni F, Barresi S, Ciolfi A, et al. (2018). Mutations in KCNK4 that Affect Gating Cause a Recognizable Neurodeveloamental Syndrome. Am J Hum Genet 103, 621–630. [PubMed: 30290154]

Bean BP (2007). The action potential in mammalian central neurons. Nat Rev Neurosci 8, 451–465. [PubMed: 17514198]

Binah O, and Palti Y (1981). Potassium channels in the nodal membrane of rat myelinated fibres. Nature 290, 598–600. [PubMed: 6261147]

Blin S, Ben Soussia I, Kim EJ, Brau F, Kang D, Lesage F, and Bichet D (2016). Mixing and matching TREK/TRAAK subunits generate heterodimeric K2P channels with unique properties. Proc Natl Acad Sci U S A 113, 4200–4205. [PubMed: 27035965]

Boullerne AI (2016). The history of myelin. Exp Neurol.

Caldwell JH, Schaller KL, Lasher RS, Peles E, and Levinson SR (2000). Sodium channel Na(v)1.6 is localized at nodes of ranvier, dendrites, and synapses. Proc Natl Acad Sci U S A 97, 5616–5620. [PubMed: 10779552]

Castelfranco AM, and Hartline DK (2015). The evolution of vertebrate and invertebrate myelin: a theoretical computational study. J Comput Neurosci 38, 521–538. [PubMed: 25832903]

Castelfranco AM, and Hartline DK (2016). Evolution of rapid nerve conduction. Brain Res 1641, 11–33. [PubMed: 26879248]

Chang W, Kanda H, Ikeda R, Ling J, DeBerry JJ, and Gu JG (2016). Merkel disc is a serotonergic synapse in the epidermis for transmitting tactile signals in mammals. Proc Natl Acad Sci U S A 113, E5491–5500. [PubMed: 27573850]

Chiu SY, and Ritchie JM (1980). Potassium channels in nodal and internodal axonal membrane of mammalian myelinated fibres. Nature 284, 170–171. [PubMed: 6244497]

Devaux J, Alcaraz G, Grinspan J, Bennett V, Joho R, Crest M, and Scherer SS (2003). Kv3.1b is a novel component of CNS nodes. J Neurosci 23, 4509–4518. [PubMed: 12805291]

Devaux JJ, Kleopa KA, Cooper EC, and Scherer SS (2004). KCNQ2 is a nodal K+ channel. J Neurosci 24, 1236–1244. [PubMed: 14762142]

Devaux JJ, Odaka M, and Yuki N (2012). Nodal proteins are target antigens in Guillain-Barre syndrome. J Peripher Nerv Syst 17, 62–71. [PubMed: 22462667]

Enyedi P, and Czirjak G (2010). Molecular background of leak K+ currents: two-pore domain potassium channels. Physiol Rev 90, 559–605. [PubMed: 20393194]

Franz DN, and Iggo A (1968). Conduction failure in myelinated and non-myelinated axons at low temperatures. J Physiol 199, 319–345. [PubMed: 5723515]

Goldstein SA, Bayliss DA, Kim D, Lesage F, Plant LD, and Rajan S (2005). International Union of Pharmacology. LV. Nomenclature and molecular relationships of two-P potassium channels. Pharmacol Rev 57, 527–540. [PubMed: 16382106]

Gottschaldt KM, Iggo A, and Young DW (1973). Functional characteristics of mechanoreceptors in sinus hair follicles of the cat. J Physiol 235, 287–315. [PubMed: 4763992]

Halter JA, and Clark JW Jr. (1993). The influence of nodal constriction on conduction velocity in myelinated nerve fibers. Neuroreport 4, 89–92. [PubMed: 8384020]

Hodgkin AL, and Huxley AF (1952). The dual effect of membrane potential on sodium conductance in the giant axon of Loligo. J Physiol 116, 497–506. [PubMed: 14946715]

Hucho F, Bergman C, Dubois JM, Rojas E, and Kiefer H (1976). Selective inhibition of potassium conductance in node of Ranvier with a photoaffinity label derived from tetraethylammonium. Nature 260, 802–804. [PubMed: 1083490]

Huxley AF, and Stampfli R (1949). Evidence for saltatory conduction in peripheral myelinated nerve fibres. J Physiol 108, 315–339.

Ikeda R, Cha M, Ling J, Jia Z, Coyle D, and Gu JG (2014). Merkel cells transduce and encode tactile stimuli to drive Abeta-afferent impulses. Cell 157, 664–675. [PubMed: 24746027]

Jenkins PM, Kim N, Jones SL, Tseng WC, Svitkina TM, Yin HH, and Bennett V (2015). Giant ankyrin-G: a critical innovation in vertebrate evolution of fast and integrated neuronal signaling. Proc Natl Acad Sci U S A 112, 957–964. [PubMed: 25552556]

Kang D, Choe C, and Kim D (2005). Thermosensitivity of the two-pore domain K+ channels TREK-2 and TRAAK. J Physiol 564, 103–116. [PubMed: 15677687]

Kim Y, Bang H, Gnatenco C, and Kim D (2001). Synergistic interaction and the role of C-terminus in the activation of TRAAK K+ channels by pressure, free fatty acids and alkali. Pflugers Arch 442, 64–72. [PubMed: 11374070]

Levitz J, Royal P, Comoglio Y, Wdziekonski B, Schaub S, Clemens DM, Isacoff EY, and Sandoz G (2016). Heterodimerization within the TREK channel subfamily produces a diverse family of highly regulated potassium channels. Proc Natl Acad Sci U S A 113, 4194–4199. [PubMed: 27035963]

Li J (2015). Molecular regulators of nerve conduction - Lessons from inherited neuropathies and rodent genetic models. Exp Neurol 267, 209–218. [PubMed: 25792482]

Lillie RS (1925). Factors Affecting Transmission and Recovery in the Passive Iron Nerve Model. J Gen Physiol 7, 473–507. [PubMed: 19872151]

Liu PW, Blair NT, and Bean BP (2017). Action Potential Broadening in Capsaicin-Sensitive DRG Neurons from Frequency-Dependent Reduction of Kv3 Current. J Neurosci 37, 9705–9714. [PubMed: 28877968]

Lotshaw DP (2007). Biophysical, pharmacological, and functional characteristics of cloned and native mammalian two-pore domain K+ channels. Cell Biochem Biophys 47, 209–256. [PubMed: 17652773]

Maingret F, Lauritzen I, Patel AJ, Heurteaux C, Reyes R, Lesage F, Lazdunski M, and Honore E (2000). TREK-1 is a heat-activated background K(+) channel. EMBO J 19, 2483–2491. [PubMed: 10835347]

Maingret F, Patel AJ, Lesage F, Lazdunski M, and Honore E (1999). Mechano- or acid stimulation, two interactive modes of activation of the TREK-1 potassium channel. J Biol Chem 274, 26691–26696. [PubMed: 10480871]

Mirkovic K, Palmersheim J, Lesage F, and Wickman K (2012). Behavioral characterization of mice lacking Trek channels. Front Behav Neurosci 6, 60. [PubMed: 22973213]

Moore JW, Joyner RW, Brill MH, Waxman SD, and Najar-Joa M (1978). Simulations of conduction in uniform myelinated fibers. Relative sensitivity to changes in nodal and internodal parameters. Biophys J 21, 147–160. [PubMed: 623863]

Ranvier L-A (1871). Contributions à l'histologie et à la physiologie des nerfs périphériques. Comptes Rendus de l'Académie des Sciences 73, 1168–1171.

Ranvier L (1872). Recherches sur l'histologie et la physiologie des nerfs. 4, 129–149.

Rash JE, Vanderpool KG, Yasumura T, Hickman J, Beatty JT, and Nagy JI (2016). KV1 channels identified in rodent myelinated axons, linked to Cx29 in innermost myelin: support for electrically active myelin in mammalian saltatory conduction. J Neurophysiol 115, 1836–1859. [PubMed: 26763782]

Renigunta V, Schlichthorl G, and Daut J (2015). Much more than a leak: structure and function of K(2)p-channels. Pflugers Arch 467, 867–894. [PubMed: 25791628]

Rhodes KJ, Strassle BW, Monaghan MM, Bekele-Arcuri Z, Matos MF, and Trimmer JS (1997). Association and colocalization of the Kvbeta1 and Kvbeta2 beta-subunits with Kv1 alpha-subunits in mammalian brain K+ channel complexes. J Neurosci 17, 8246–8258. [PubMed: 9334400]

Ritchie JM, and Rogart RB (1977). Density of sodium channels in mammalian myelinated nerve fibers and nature of the axonal membrane under the myelin sheath. Proc Natl Acad Sci U S A 74, 211–215. [PubMed: 299947]

Royal P, Andres-Bilbe A, Avalos Prado P, Verkest C, Wdziekonski B, Schaub S, Baron A, Lesage F, Gasull X, Levitz J, et al. (2019). Migraine-Associated TRESK Mutations Increase Neuronal Excitability through Alternative Translation Initiation and Inhibition of TREK. Neuron 101, 232–245 e236. [PubMed: 30573346]

Stathopoulos P, Alexopoulos H, and Dalakas MC (2015). Autoimmune antigenic targets at the node of Ranvier in demyelinating disorders. Nat Rev Neurol 11, 143–156. [PubMed: 25623793]

Tasaki I (1939). The electro-saltatory transmission of the nerve impulse and the effect of narcosis upon the nerve fiber. J Physiol-London 127, 211–227.

Waddell PJ, and Lawson SN (1990). Electrophysiological properties of subpopulations of rat dorsal root ganglion neurons in vitro. Neuroscience 36, 811–822. [PubMed: 2234413]

Waxman SG (1992). Demyelination in spinal cord injury and multiple sclerosis: what can we do to enhance functional recovery? J Neurotrauma 9 Suppl 1, S105–117. [PubMed: 1588601]

Waxman SG (2006). Axonal conduction and injury in multiple sclerosis: the role of sodium channels. Nat Rev Neurosci 7, 932–941. [PubMed: 17115075]

Zhou L, Messing A, and Chiu SY (1999). Determinants of excitability at transition zones in Kv1.1-deficient myelinated nerves. J Neurosci 19, 5768–5781. [PubMed: 10407018]

Highlights

TREK-1 and TRAAK are clustered at nodes of Ranvier of myelinated afferent nerves.

They are required for rapid action potential (AP) regeneration at nodes of Ranvier.

They permit high-speed and high-frequency AP conduction on the afferent nerves.

Suppressing these channels retards nerve conduction and impairs sensory functions.

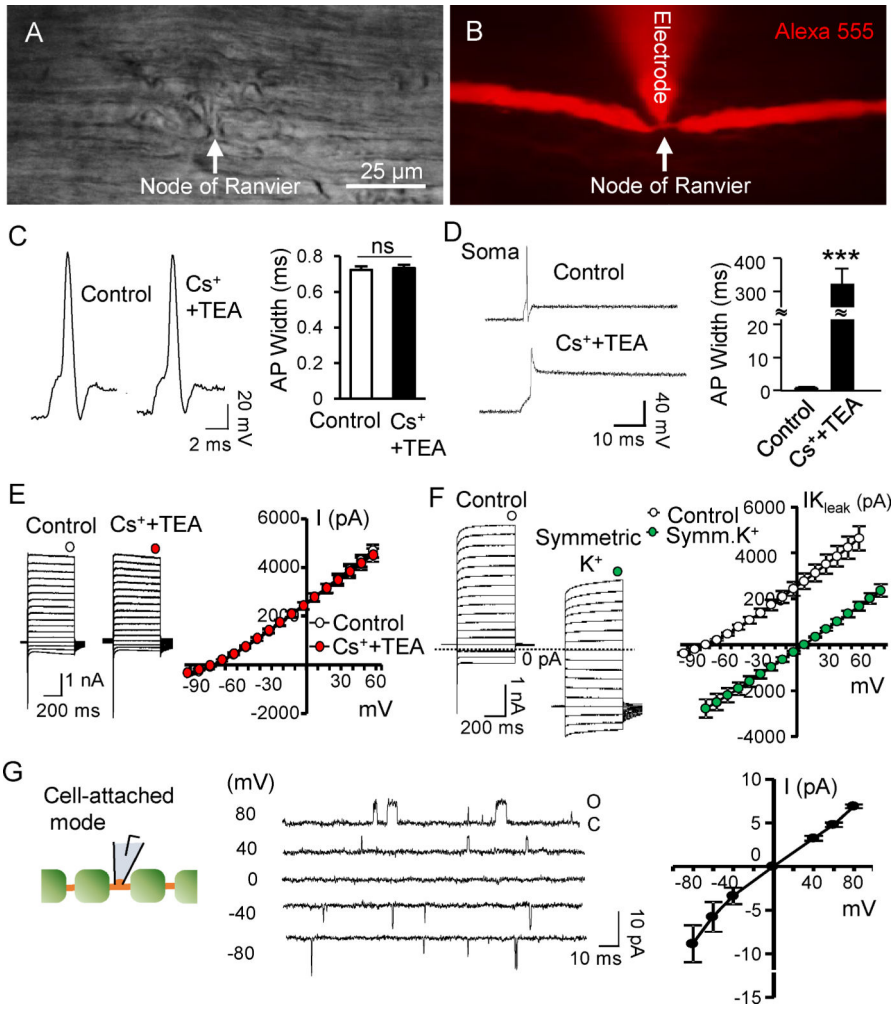

Figure 1. Nodes of Ranvier of myelinated afferent nerves display unconventional action potentials and high leak K^+ conductance.

A) *Ex-vivo* trigeminal afferent nerve preparation. **B)** Fluorescent image shows patch-clamp recordings at a node of Ranvier (NR) of a trigeminal Aβ-afferent nerve. The electrode contained Alexa-555 to trace the NR (arrow indicated) and other axonal regions. **C)** Traces illustrate typical action potentials (APs) recorded at NRs in the absence (control, left) and presence of the voltage-gated K^+ channel blockers of intracellular 135 mM Cs^+ plus extracellular 20 mM TEA (Cs^++TEA, right). Bar graph shows widths of APs at NRs in the absence (control, n = 9) and presence of Cs^++TEA (n = 11). **D**) Traces illustrate APs recorded from a soma of a trigeminal Aβ-afferent nerve in the absence (top, control) and presence of Cs^++TEA (bottom). Bar graph shows AP widths in the absence (control, n = 7) and presence of Cs^++TEA (n = 6). **E**) Traces illustrate currents recorded at NRs following voltage steps in the absence (left, control) and presence of Cs^++TEA (right). Right panel, I-V curves of non-inactivating currents in control (n = 9) and the presence of Cs^++TEA (n = 9). **F**) Traces illustrate non-inactivating currents at NRs following voltage steps in control with $[K^+]_{out}/[K^+]_{in}$ = 5 mM/135 mM (left) and symmetric K^+ with $[K^+]_{out}/[K^+]_{in}$ = 135 mM/135 mM (right). Right panel, I-V curves of non-inactivating currents recorded at NRs in control (n = 7) and symmetrical K^+ (n = 7). **G**) Left, recording setting. Middle, traces

illustrate IK_{leak} single channel currents at different voltages across the nodal membrane patch. Right, I-V curve of IK_{leak} single channel currents recorded at NRs (n = 15). Data represent Mean ± SEM, ns, not significantly different, ***$p < 0.001$, Student's t-Test. See also Fig. S1–4, Table S1

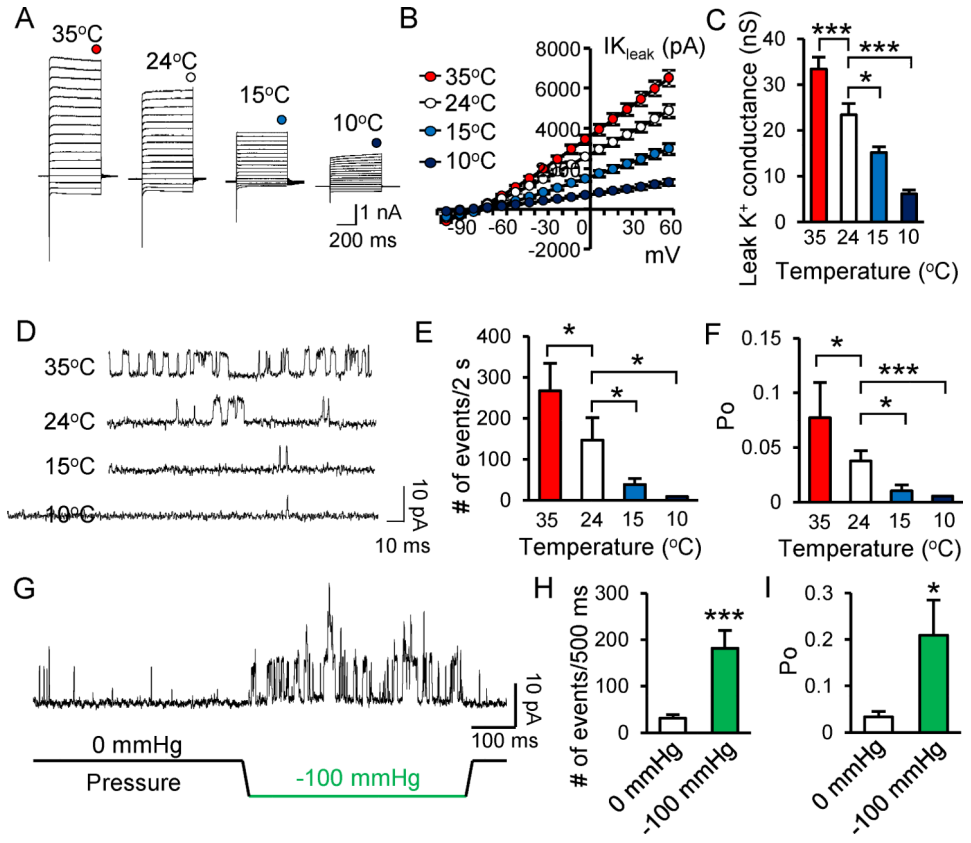

Figure 2. Leak K$^+$ conductance at nodes of Ranvier of myelinated afferent nerves are thermosensitive and mechanosensitive channels.

A-C) Sample traces (**A**), I-V curves (**B**), whole-cell conductance (**C**) of IK_{leak} recorded at NRs at 35°C (n = 8), 24°C (control, n = 8),15°C (n = 8), and 10°C (n = 6). IK_{leak} conductance is the slope between − 72 to −82 mV in I-V curves. Recordings were made in whole-cell mode. **D-F**) Sample traces of IK_{leak} single channel activity (**D**), summary (n = 6) of IK_{leak} single channel events (**E**), and open probability (**F**) recorded at 80 mV from NRs at 35, 24, 15 and 10°C. **G-I)** Sample traces of IK_{leak} single channel activity (**G**), summary (n = 6) of IK_{leak} single channel events (**H**) and open probability (**I**) recorded at 80 mV from NRs at 0 mmHg and following intra-electrode applications of −100 mmHg pressures. In **D-I**, recordings were performed under the cell-attached mode with $[K^+]_{in}/[K^+]_{out}$ of ~1. Data represent Mean ± SEM, *$p < 0.05$, ***$p < 0.001$, one-way ANOVA with the Tukey post hoc test or Student's t-Test.

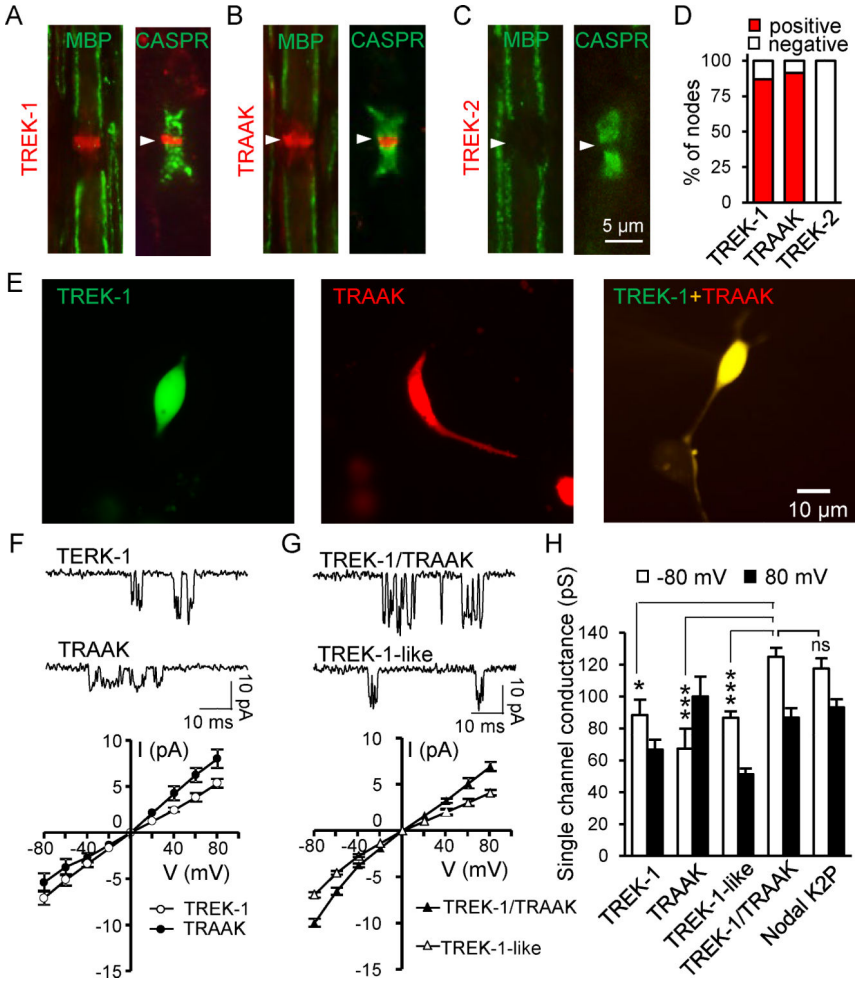

Figure 3. TREK-1 and TRAAK channels are molecular identities of leak K^+ channels at NRs of myelinated afferent nerves.

A) Left, TREK-1 immunoreactivity (TREK-1-ir) at a NR and MBP immunoreactivity (MBP-ir) on myelin sheath. Right, TREK-1-ir at a NR and CASPR-ir in paranodal regions. **B)** Left, TRAAK-ir at a NR and MBP-ir on myelin sheath. Right, TRAAK-ir at a NR and CASPR-ir in paranodal regions. **C)** Similar to A&B except TREK-2-ir was examined and was negative at NRs. In **A-C**, NRs are indicated by arrows. MBP, myelin basic protein. CASPR, contactin associated protein. **D)** Summary of immunoreactive nodes for experiments represented in **A-C**: 112/129 nodes were TREK-1-ir positive, 118/129 nodes were TRAAK-ir positive. 0/129 nodes were TREK-2-ir positive. **E)** HEK293 cells transfected with TREK-1/eGFP (left), TRAAK/mCherry (middle), and both TREK-1/EGFP and TRAAK/mCherry (right). **F)** Traces illustrate single channel currents recorded at −80 mV from an HEK293 cell transfected with TREK-1/eGFP (upper, homomeric TREK-1) or an HEK293 cell transfected with TRAAK/mCherry (lower, homomeric TRAAK). Bottom, I-V curves of single channel currents recorded at different transmembrane voltages for homomeric TREK-1 channels (open circles, n = 7) or homomeric TRAAK (solid circles, n = 6). **G)** Sample traces show two types of single channels recorded at −80 mV from a HEK293 cell co-transfected with TREK-1/eGFP and TRAAK/mCherry plasmids, one type (upper,

TREK-1/TRAAK) has unitary currents apparently larger than homomeric channels and another type (lower, TREK-1-like) has unitary currents similar to homomeric TREK-1 channels shown in F. Bottom panel, I-V curves of the currents of TREK-1/TRAAK single channels (n = 12, solid triangles) and TREK-1-like single channels (n = 13, open triangles). **H)** Summary of single channel conductance at −80 mV (open bars) and 80 mV (closed bars) for homomeric TREK-1 (n = 5 at −80 mV, n = 6 at 80 mV), homomeric TRAAK (n = 6 at both voltages), TREK-1-like (n = 12 at −80 mV, n = 5 at 80 mV), and TREK-1/TRAAK channels (n = 8 at −80 mV, n = 5 at 80 mV) expressed in HEK293 cells. The single channel conductance of nodal K2P channels (n = 13 at both voltages) is also included in the graph for a comparison. The single channel conductance at −80 mV was used for comparison. All recordings were performed under the cell-attached mode. Data represent Mean ± SEM, ns, no significant difference, $*p < 0.05$, $***p < 0.001$, one-way ANOVA with the Tukey post hoc test. See also Fig. S5–9

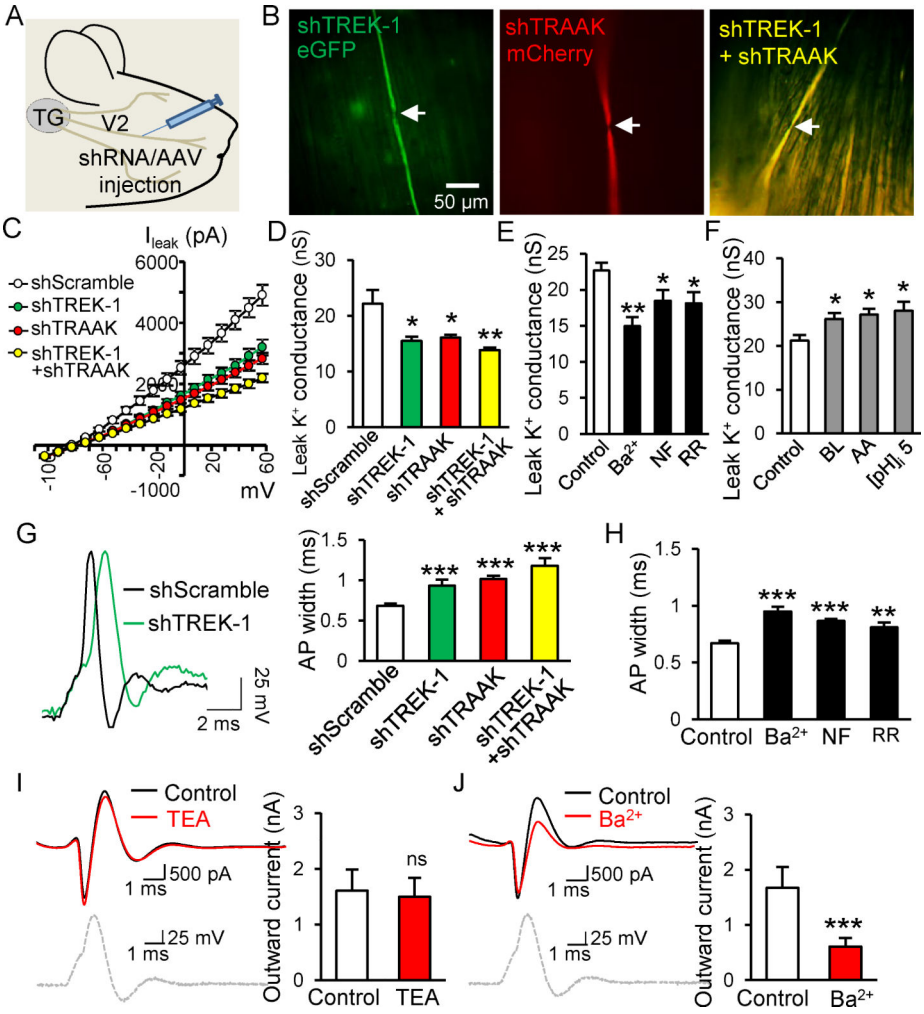

Figure 4. Genetic and pharmacological manipulation of TREK-1 and TRAAK activity reveals their roles in the formation of rapid action potentials at nodes of Ranvier of myelinated afferent nerves.

A) Illustration of intra-nerve microinjections of shRNA/AAV preparations. **B)** Axons of trigeminal Aβ-afferent nerves expressing TREK-1-shRNA/eGFP (shTREK-1, left), TRAAK-shRNA/mCherry (shTRAAK, middle), and TREK-1-shRNA/eGFP plus TRAAK-shRNA/mCherry (shTREK-1+shTRAAK, right) 30 days after *in vivo* shRNA/AAV microinjections. Arrow in each panel indicates a NR. **C)** I-V curves of whole-cell IK_{leak} recorded at NRs of shScramble (n = 7), shTREK-1 (n = 6), shTRAAK (n = 6), and shTREK-1+shTRAAK (n = 6) groups. **D)** IK_{leak} conductance at NRs of shScramble (n = 7), shTREK-1 (n = 6), shTRAAK (n = 7), and shTREK-1+shTRAAK (n = 6) groups. **E)** IK_{leak} conductance at NRs in control (n = 9), the presence of 5 mM Ba^{2+} (n = 15), 50 μm norfluoxetine (NF, n = 6) and 2 μm ruthenium red (RR, n = 10). **F)** IK_{leak} conductance at NRs in control (n = 8), the presence of 10 μm BL 1249 (BL, n = 9), intracellular 20 μm arachidonic acid (AA, n = 9) and intracellular pH of 5 ($[pH]_i$ 5, n = 10). **G)** Left, traces illustrate APs recorded at NRs of shScramble and shTREK-1 groups. Right, AP widths in shScramble (n = 7), shTREK-1 (n = 6), shTRAAK (n = 6), and shTREK-1+shTRAAK (n = 6) groups. **H)** AP widths at NRs before (control, n = 9), following the applications of 5 mM

Ba^{2+} (n = 15), 50 μm NF (n = 6), or 2 μm RR (n = 10). **I)** Left, traces on top illustrate currents recorded at NRs under AP-dynamic clamp mode before (control) and following 20 mM TEA application. The trace on the bottom was the AP waveform for AP-dynamic clamp. Right, summary of outward currents at NRs during AP repolarization phase before (n = 6) and following TEA application. **J)** Left, traces on the top illustrate currents recorded at NRs under AP-dynamic clamp mode before (control) and following 5 mM Ba^{2+} application. The trace on the bottom was the AP waveform for AP-dynamic clamp. Right, summary of outward currents recorded at NRs during AP repolarization before (n = 6) and following Ba^{2+} application. Data represent Mean ± SEM, ns, not significantly different, * $p < 0.05$, ** $p < 0.01$, *** $p < 0.001$, one-way ANOVA with the Tukey post hoc test or Student's t-Test. See also Fig. S10–12, Table S2.

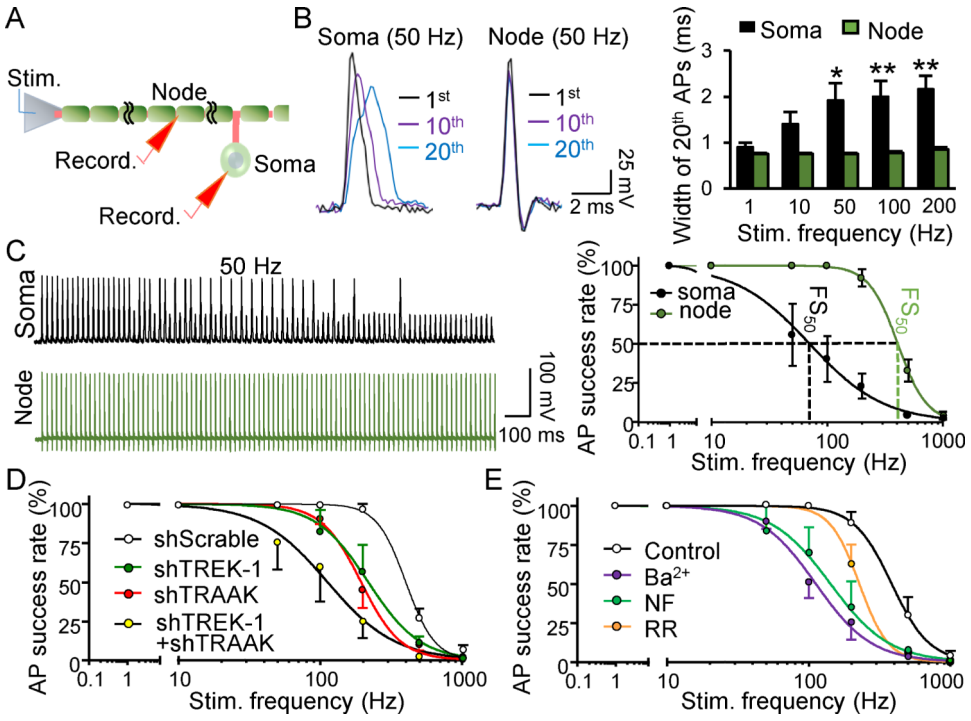

Figure 5. TREK-1 and TRAAK channels are required for high-frequency saltatory conduction on myelinated afferent nerves.

A) Experimental setting. **B)** Traces illustrate APs recorded from the soma (left) and NR (right) of a trigeminal Aβ-afferent nerve following 50 Hz stimulation. Traces were 1st, 10th and 20th APs. Bar graph, AP widths of 20th APs at somas (n = 7, black) or NRs (n = 7, green) following stimulation at 1 to 200 Hz. Stimulation duration, 20 s. **C)** Left, two traces illustrate APs recorded at a soma (top) and a NR (bottom) following stimulation at 50 Hz. Tall spikes, successful APs. Right, AP success rates at somas (n = 7) and NRs (n = 7) with stimulation from 1 to 1000 Hz. Dashed lines indicate the frequency at which AP conduction success rate is 50% (FS_{50}). **D)** AP success rates at NRs of shScramble (n = 6), shTREK-1 (n = 6), shTRAAK (n = 6), and shTREK-1+shTRAAK (n = 6) groups. **E)** AP success rates at NRs before (control, n = 6), following application of 5 mM Ba^{2+} (n = 7), 50 μm NF (n = 6), or 2 μm RR (n = 6). Recording duration at each frequency was 20 s. Data represent Mean ± SEM, * $p < 0.05$, ** $p < 0.01$, one-way ANOVA with the Tukey post hoc test. See also Fig. S13&14.

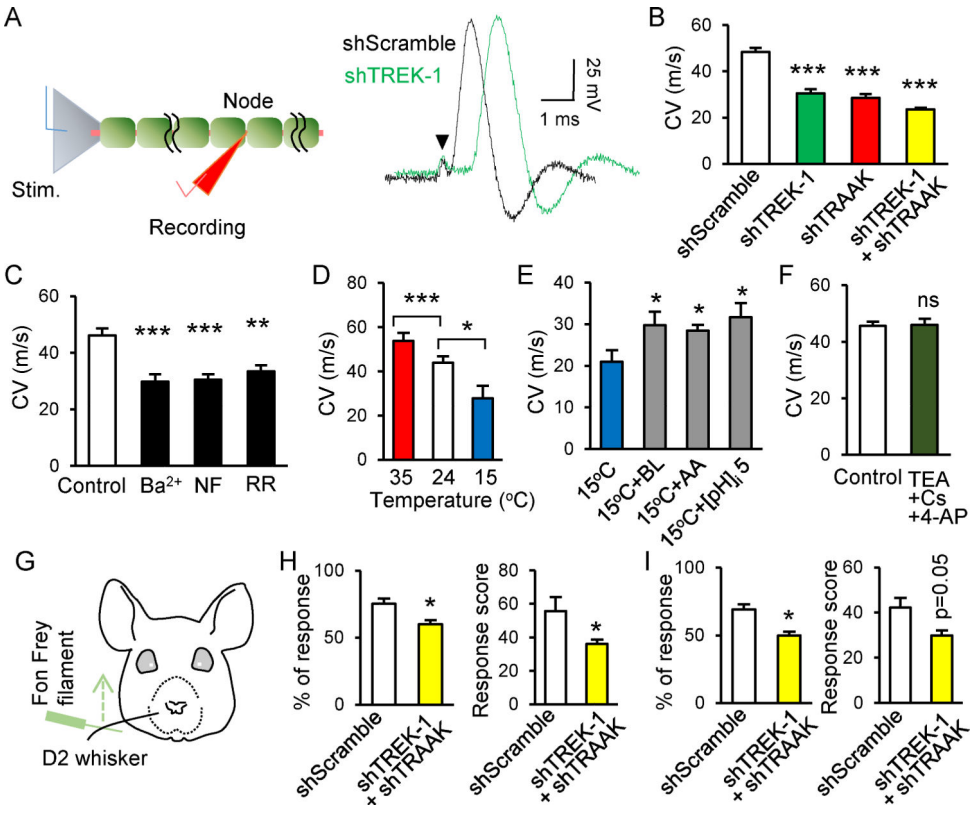

Figure 6. TREK-1 and TRAAK channels at nodes of Ranvier of myelinated afferent nerves are required for high-speed saltatory conduction and for sensory behavioral responses.

A) Left, experimental setting. Right, traces illustrate APs recorded at NRs of shScramble and shTREK-1 groups. Arrow indicates stimulation marks. **B)** AP conduction velocity (CV) in shScramble (n = 6), shTREK-1 (n = 6), shTRAAK (n = 6), and shTREK-1+shTRAAK groups (n = 6). **C)** CV in the absence (control, n = 6), present of 5 mM Ba^{2+} (n = 7), 50 μm NF (n = 6), and 2 μm RR (n = 6). **D)** CV (n = 7) at NRs at 35°C, 24°C, and 15°C. **E)** CV at NRs at 15°C without (n = 8), and with 10 μm BL (n = 7), 20 μm AA (n = 6), and intracellular pH of 5 ($[pH]_i$ 5, n = 6). AA and $[pH]_i$ 5 were applied intracellularly via recording electrodes. **F)** CV recorded at NRs in the absence (control, n = 8) and presence (n = 8) of voltage-gated K^+ channel blockers TEA (20 mM, extracellular), Cs^+(135 mM, intracellular), plus 4-AP (1 mM, intracellular). **G)** Diagram illustrates whisker tactile test. **H)** Percentage (left) and scores (right) of whisker tactile responses in animals 30 days after microinjection of shScramble (n = 6) and shTREK-1+shTRAAK (n = 6) into D2 whisker hair follicles. **I)** Percentage (left) and scores (right) of whisker tactile responses in animals 30 days after intra-nerve microinjection of shScramble (n = 6) and shTREK-1 + shTRAAK (n = 6) into D2 whisker nerve branches. Data represent Mean ± SEM, $*p < 0.05$, $**p < 0.01$, $***p < 0.001$, one-way ANOVA with the Tukey post hoc test or Student's t-Test.

KEY RESOURCES TABLE

REAGENT or RESOURCE	SOURCE	IDENTIFIER
Antibodies		
Rabbit anti-K2P 2.1 (TREK-1)	Alomone	APC-047, lot #AN03
		APC-047, lot #AN062
		APC-047, lot #AN0550
Rabbit anti-K2P 10.1 (TREK-2)	Alomone	APC-055, lot #AN01
Rabbit anti-K2P 4.1 (TRAAK)	Alomone	APC-108, lot #AN02
Chicken anti-Myelin basic protein	Abcam	Ab134018
Mouse monoclonal anti-CASPR	MilliporeSigma	MABN69, lot 3116292
Chicken anti-GFP	Aves Labs Inc	GFP-1010
Mouse anti-mCherry	Abcam	Ab125096
Alexa Fluor 594-conjugated goat anti-rabbit	Invitrogen	A-11012
Alexa Fluor 488-conjygated goat anti-rabbit	Invitrogen	A-11008
Alexa Fluor 594-conjugated goat anti-mouse	Invitrogen	A-11032
Alexa Fluor 488-conjugated goat anti-mouse	Invitrogen	A-11029
Alexa Fluor 488-conjugated goat anti-chicken	Abcam	AB 150169
Chemicals, Peptides, and Recombinant Proteins		
Isoflurane	Vet One	V1-502017
Tetraethylammonium	MilliporeSigma	T2265
Cesium chloride	MilliporeSigma	C3139
4-pyridinamine	MilliporeSigma	A78403
Barium chloride	MilliporeSigma	B0750
Ruthenium red	MilliporeSigma	R2751
Norfluoxetine	Cayman Chemical	15900
BL1249	Tocris Bioscience	3797
Arachidonic acid	Tocris Bioscience	2756
Ionomycin	MilliporeSigma	I9657
Linopirdine	Tocris Bioscience	1999
Zinc chloride	MilliporeSigma	Z4875
Phoretin	MilliporeSigma	P7912
4,4’-Diisothiocyanato-2,2’-stilbenedisulfonic acid disodium salt (DIDS)	Tocris Bioscience	4523
Alexa Fluor 555	ThermoFisher Scientific	A20501MP
Paraformaldehyde (PFA)	Sigma	P6148
Dispase® II	Roche	11534200
Collagenase	MilliporeSigma	C0130
Goat serum	Jackson Immuno Research	005-000-121
PBS	ThermoFisher Scientific	28374
Antifade Mountant	ThermoFisher Scientific	P36965
Lipofectamine 2000	Invitrogen	11668-027
DMEM	Fisher Scientific	10-013-CV

REAGENT or RESOURCE	SOURCE	IDENTIFIER
Fetal bovine serum	Hyclone/Fisher Scientific,	SH30071.02
Penicillin-streptomycin	Invitrogen	15140-122
Acetone	ThermoFisher Scientific	A18-500
K2P 2.1(TREK-1) 8-25 Peptide	Alomone	APC047AG0340
K2P 4.1 (TRAAK) 343-359 Peptide	Alomone	APC108AG0240
Experimental Models: Organisms/Strains		
Sprague-Dawley rats	Envigo	Hsd:Sprague Dawley® SD®
HEK293	ATCC	CRL1513
Oligonucleotides		
5'- CAAAGTGGAGGACACATTTAT-3' (shRNA for TREK-1)	VectorBuilder	https://en.vectorbuilder.com
5'-ACCATCGGCTACGGCAATATA-3' (shRNA for TRAAK)	VectorBuilder	https://en.vectorbuilder.com
5'-CCTAAGGTTAAGTCGCCCTCG-3' (scrambled shRNA)	VectorBuilder	https://en.vectorbuilder.com
Recombinant DNA		
rKcnk2 (TREK-1) <	VectorBuilder	NM_172042.1
rKcnk4 (TRAAK)	VectorBuilder	NM_053804.2
pAAV[shRNA]-mCherry-U6	VectorBuilder	VB170731–1050hzr
pAAV[shRNA]-eGFP-U6	VectorBuilder	VB170731–1048udv
pRP[Exp]-eGFP-CMV	VectorBuilder	VB180907–1066wfg
pRP[Exp]-mCherry-CMV	VectorBuilder	VB180907–1065krm
Virus Strains		
AAV5 particles	VectorBuilder	https://en.vectorbuilder.com
AAV2 particles	VectorBuilder	https://en.vectorbuilder.com
Software and Algorithms		
pCLAMP10	Molecular Devices	www.moleculardevices.com
Metaflour	Molecular Devices	www.moleculardevices.com
Prism	GraphPad	www.graphpad.com
Other		
Olympus BX50	Olympus	www.olympus-lifescience.com
Axopatch 200B	Molecular Devices	www.moleculardevices.com
Master-8 Stimulator	A.M.P.I	www.ampi.co.il
High-speed pressure-clamp device	ALA Scientific instruments	https://alascience.com/
Leica CM1860 cryomicrotome	Leica Biosystems	www.leicabiosystems.com